



UNIVERSITY OF LEEDS

This is a repository copy of *Hybrid event beds in the proximal to distal extensive lobe domain of the coarse-grained and sand-rich Bordighera turbidite system (NW Italy)*.

White Rose Research Online URL for this paper:
<http://eprints.whiterose.ac.uk/118682/>

Version: Accepted Version

Article:

Mueller, P, Patacci, M orcid.org/0000-0003-1675-4643 and Di Giulio, A (2017) Hybrid event beds in the proximal to distal extensive lobe domain of the coarse-grained and sand-rich Bordighera turbidite system (NW Italy). *Marine and Petroleum Geology*, 86. pp. 908-931. ISSN 0264-8172

<https://doi.org/10.1016/j.marpetgeo.2017.06.047>

(c) 2017, Elsevier Ltd. This manuscript version is made available under the CC BY-NC-ND 4.0 license <http://creativecommons.org/licenses/by-nc-nd/4.0/>

Reuse

Items deposited in White Rose Research Online are protected by copyright, with all rights reserved unless indicated otherwise. They may be downloaded and/or printed for private study, or other acts as permitted by national copyright laws. The publisher or other rights holders may allow further reproduction and re-use of the full text version. This is indicated by the licence information on the White Rose Research Online record for the item.

Takedown

If you consider content in White Rose Research Online to be in breach of UK law, please notify us by emailing eprints@whiterose.ac.uk including the URL of the record and the reason for the withdrawal request.

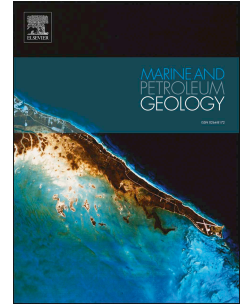


eprints@whiterose.ac.uk
<https://eprints.whiterose.ac.uk/>

Accepted Manuscript

Hybrid event beds in the proximal to distal extensive lobe domain of the coarse-grained and sand-rich Bordighera turbidite system (NW Italy)

Pierre Mueller, Marco Patacci, Andrea Di Giulio



PII: S0264-8172(17)30254-4

DOI: [10.1016/j.marpetgeo.2017.06.047](https://doi.org/10.1016/j.marpetgeo.2017.06.047)

Reference: JMPG 2981

To appear in: *Marine and Petroleum Geology*

Received Date: 16 January 2017

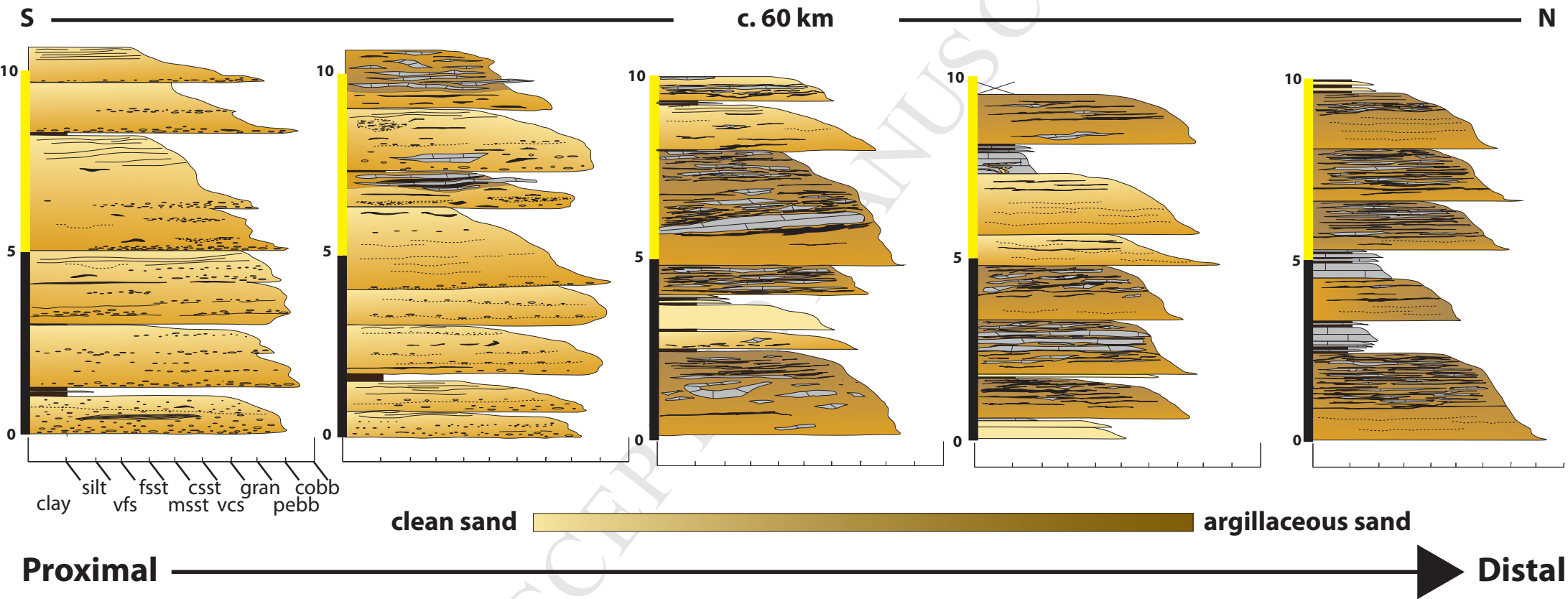
Revised Date: 20 June 2017

Accepted Date: 28 June 2017

Please cite this article as: Mueller, P., Patacci, M., Di Giulio, A., Hybrid event beds in the proximal to distal extensive lobe domain of the coarse-grained and sand-rich Bordighera turbidite system (NW Italy), *Marine and Petroleum Geology* (2017), doi: 10.1016/j.marpetgeo.2017.06.047.

This is a PDF file of an unedited manuscript that has been accepted for publication. As a service to our customers we are providing this early version of the manuscript. The manuscript will undergo copyediting, typesetting, and review of the resulting proof before it is published in its final form. Please note that during the production process errors may be discovered which could affect the content, and all legal disclaimers that apply to the journal pertain.

Idealized down-current axial sediment fairway stacking patterns



Hybrid event beds in the proximal to distal extensive lobe domain of the coarse-grained and sand-rich Bordighera turbidite system (NW Italy)

Pierre Mueller^{1*}, Marco Patacci², Andrea Di Giulio¹

¹ Dipartimento di Scienze della Terra e dell'Ambiente, Università di Pavia, Pavia, Italy.

² Turbidites Research Group, School of Earth and Environment, University of Leeds, Leeds, LS2 9JT, United Kingdom.

- Corresponding author
- Email-address: pierre.mueller01@universitadipavia.it (P. Mueller)

Abstract

The Upper Cretaceous Bordighera Sandstone of NW Italy is a coarse-grained, sand-rich elongated turbidite system (ca. 15 x 45 km in outcrop) up to 250 meters thick, interpreted to have been deposited in a trench setting. The siliciclastic succession interfingers with muddy calcareous turbidites, which become more abundant toward the lateral and distal domains. Bed type associations allow the distinction of a proximal channelized domain which transitions to a more distal lobe domain, characterized by abundant mudclast-rich sandstones and by bipartite and tripartite beds with a mud-rich middle or upper division (hybrid event beds). The transition between the proximal and distal domains occurs over a relatively limited spatial extent (ca. 5 km). The presence of lenticular bed-sets made up of coarse grained and mud-poor sandstones throughout the distal domain suggests that distributary channels were present, indicating sediment bypass further down-dip toward the most distal and not preserved parts of the system. Hybrid event beds - commonly associated with distal and marginal fan environments such as fan fringes - are present throughout the lobe domain and extend for up to ca. 30 km in down-dip distance. They are more abundant in the proximal and axial depositional lobe domain and their appearance occurs within a short basin-ward distance from the inferred channel-lobe transition zone. Flow expansion at the termination of the channelized domain and the enhanced availability of cohesive substrate due to the presence of intra-basinal muddy calcareous beds are interpreted as the key controls on pronounced argillaceous sandstone distribution. The abrupt appearance and the persistent occurrence of such beds across an extensive domain have implications for characterizing bed-scale (sub-seismic) heterogeneity of deep-water clastic hydrocarbon reservoirs.

Keywords: sand-rich turbidite system, bed-scale heterogeneity, hybrid event beds, hyperconcentrated density flows, degree of flow confinement

1. Introduction

The sediment gravity flow spectrum is traditionally regarded as comprising two end-members, namely cohesive

flows (debris flows) and frictional flows (turbidity currents) (e.g. Lowe, 1982; Mulder & Alexander, 2001; Talling et al., 2012). Yield strength and grain interactions account for the dominant particle support mechanisms in debris flows, whereas the primary supporting mechanism of turbidity currents is represented by fluid turbulence (Sumner et al., 2009). In recent years, research efforts have been directed at better understanding flow states intermediate between the two end-members and that share both laminar and turbulent flow properties (e.g. Baas et al., 2009; Southern et al., 2015). Flume experiments (e.g. Baas et al., 2009; 2011) reveal that the concentration of clay within the flow plays a crucial role on emerging rheological flow heterogeneity as it dampens turbulence. Deposits that record both or intermediate flow characteristics commonly comprise a roughly two-part arrangement of a lower mud-poor sandstone portion and an upper mud-rich sandstone and have been documented in numerous studies from various settings (e.g. “slurry flows” of Lowe & Guy, 2000 and Sylvester & Lowe, 2004; “linked debrites” of Haughton et al., 2003; “hybrid event beds” of Haughton et al., 2009; “transitional flow deposits” of Kane & Pontén, 2012; “matrix-rich sandstones” of Terlaky & Arnott, 2014). As bed-scale heterogeneity has a negative impact on both lateral and vertical sandstone permeability, the occurrence of such deposits can result in sudden and unexpected reduced hydrocarbon production efficiency (e.g. Sylvester & Lowe, 2004; Amy et al., 2009; Fonnesu et al., 2015; Porten et al., 2016). Consequently, in the last decade studies on turbidite systems prone to this type of bed-scale heterogeneity increasingly came to the center of attention of both academic and applied research.

Hybrid event beds (HEBs) are a type of deposits characterized by the presence of a mud-rich division sandwiched between clean sandstone divisions (Haughton et al., 2009), resulting in a reduced primary porosity and permeability in comparison to classic turbidite sandstones. This enhanced mud content is interpreted to result from progressive clay entrainment during flow evolution (see also Haughton et al., 2003; Amy & Talling, 2007; Davis et al., 2009; Fonnesu et al., 2016). According to Haughton et al. (2009), the idealized deposit of such beds displays five divisions that tend to show variable individual thicknesses. A basal, structureless graded or ungraded sandstone (H1) that gradually passes into a banded sandstone (H2) which exhibits alternating cleaner paler sands and darker argillaceous sandstone bands, a chaotic, debritic argillaceous sandstone subdivision (H3) with variable concentrations of mud clasts and sheared sand patches, a fine grained, laminated mud-poor sandstone (H4) and a clayey mudstone cap (H5). Nevertheless, a single event bed does not necessarily comprise all of the mentioned divisions (e.g. Talling et al., 2012; Fonnesu et al., 2017).

Hybrid event beds and other deposits characterized by an argillaceous sandstone division have largely been reported from distal environments of tectonically active lobe-dominated sand-rich and mud-rich submarine fans (e.g. Haughton et al., 2009; Hodgson et al., 2009; Muzzi Magalhaes & Tinterri, 2010; see review in Fonnesu et al., 2015). Moreover, hybrid event beds have been documented in proximity to basin margins, where flows are interpreted to decelerate rapidly through interaction with the laterally confining slopes (e.g., Barker et al.,

2008; Patacci et al., 2014). Nonetheless, the occurrence of such beds has also been recognized in more proximal environments of largely unconfined turbidite systems, specifically in channelized realms located at the toe of slope of deep-sea fans (Henstra et al., 2016) or in the immediate downstream vicinity of the channel-lobe transition zone (Terlaky & Arnott, 2014).

This paper presents data on the Upper Cretaceous Bordighera Sandstone (BGS) in order to improve understanding on spatial trends in facies heterogeneity and grain size distributions in high net-to-gross turbidite systems. In particular, the present study aims to provide insights into hybrid event bed development in a sand-rich turbidite systems deposited in a subduction trench scenario prior to continental collision. The bed-scale reservoir heterogeneity linked to the presence of hybrid event beds is expected to occur below typical seismic resolution. Comprehensive outcrop studies are therefore of particular relevance in order to advance models regarding the vertical and lateral spatial distribution of facies heterogeneity in hydrocarbon reservoirs which cannot be captured by analysis of seismic datasets.

2. Background geology

The Upper Cretaceous Bordighera Sandstone (BGS) crops out in northwest Italy (Fig. 1 A-C) and is part of the San Remo-Monte Saccarello Unit of the Cretaceous-Paleocene Helminthoid Flysch Complex of the Penninic Nappe stack of the Western Ligurian Alps (Maino et al., 2012; 2014; Decarlis et al., 2013). Deep-marine sediments of the Helminthoid Flysch accumulated in the Piedmont-Ligurian oceanic basin (Vanossi et al., 1986). The Helminthoid Flysch succession became progressively incorporated into an Upper Cretaceous-Paleogene accretionary prism (Di Giulio, 1992) that finally became involved in the Ligurian Alps collisional system.

Four main units constitute the Western Ligurian Flysch complex with the San Remo-Monte Saccarello Unit representing the topmost. The chronostratigraphic organization of these units, divided by southward dipping thrusts with the oldest unit resting on top of the nappe pile, documents the typical tectonic inversion shown by accretionary wedges (Di Giulio, 1992). While the three lowermost and younger units underwent multi-phase ductile-brittle deformation, the oldest topmost San Remo-Monte Saccarello Unit is characterized by a rather simple structural overprint denoted by relatively large-scale, open SW-verging kink folds causing a tectonic shortening of roughly 30 per cent, according to available maps and structural data (Giammarino et al., 2010; Maino et al., 2012).

The San Remo-Monte Saccarello Unit is composed of three formations (Fig. 1D). The lowermost is the Upper Hauterivian to Upper Campanian San Bartolomeo Formation (SBF), a thin-bedded and very fine-grained turbidite unit (Cobianchi, et al., 1991; Galbiati & Cobianchi, 1998). This is overlain by the Bordighera Sandstone (BGS), mainly consisting of medium- to thick-bedded, coarse- to medium-grained siliciclastic turbidites (Sagri, 1980) and which constitutes the focus of this paper. Finally, the succession is capped by the San Remo Flysch

(SRF), partially heterotopic with the Bordighera Sandstone and primarily made up of medium- to thick- bedded, fine-grained calcareous turbidites featuring the characteristic Helmithoid-type ichnofossils. According to Sagri et al. (1980), the San Remo Flysch was deposited within an abyssal environment below the carbonate compensation depth.

3. Methodology

The study is based on sedimentological investigation of 10 sections along an arcuate SW-NW transect (see Fig. 1C), along the inferred main sediment transport direction. Sedimentological features were examined by detailed graphic logs (measured with 1 cm resolution and drawn at 1:50 scale) with roughly 1600 beds measured and described (ca. 1400 m in total thickness). A high-precision Jacob's staff (Patacci, 2016) was used to improve accuracy of measurements of some covered intervals. Maximum and mean grain sizes were determined in the field with a standard grain size chart and a hand lens. Measurements of paleocurrent indicators were also undertaken (groove marks, flute casts and ripples; $n = 107$). An ad-hoc bed type classification was developed, with special emphasis on mudclast-rich and argillaceous sandstone beds. Field estimations on the amount of mud dispersed within sandstones were performed on the basis of rock color and weathered surface texture. As the present day distance between measured sections is less than the distance at the time of deposition due to SSW'-NNE' directed tectonic shortening of about 30 % (Maino & Seno, 2016), restored distances were computed. Outcropping dimensions of the preserved part of the system are 15 km cross-current by ca. 45 km along-current, striking roughly parallel to the orientation of tectonic shortening. In order to restore different sections to their relative depositional position, the distances between sections along the SSW'-NNE' part of the transect were increased by 30%, resulting in an estimated extension of the exposed part of the system to ca. 15 km x 60 km.

Bed type proportions were calculated and plotted using MS Excel and Matlab. Amalgamated interval proportions (amalgamation ratio) were also computed. Amalgamated intervals were defined as sandstone intervals characterized internally by multiple (at least one) sand-on-sand contacts outlined by abrupt grain size breaks and bounded at their lower and upper boundaries by a thin clay or fine silt interval. They can be compared to the bed-sets defined by an absence of mudcaps of Stanbrook et al. (2015). The amalgamation ratio for a stratigraphic section was calculated as the ratio of the thickness of all the amalgamated sandstone intervals to the entire stratigraphic thickness. This parameter helped refine the inferred position of individual sections with respect to the axis of the siliciclastic sediment pathway (e.g. Romans et al., 2009; Pringle et al., 2010) and to discriminate in between channelized and unchannelized depositional environments (Mattern, 2002).

4. Bed types

Six main bed types comprising thirteen sub-categories have been distinguished. Their main features are summarized in Table 1. Descriptive and interpretive schemes of bed types conform to the criteria proposed by Lowe (1982), Mulder and Alexander (2001), Baas et al. (2009), Haughton et al. (2009) and Southern et al. (2016), facilitating the deduction of properties of sediment density flows (i.e., sediment concentration, particle support mechanism, types of particles and flow duration) from the characteristics of the deposit. Bed types 1 and 2 are interpreted as representing the coarse-grained depositional spectrum of sandy siliciclastic sediment density flows. Bed types 3 and 4 are interpreted to represent deposits of flows transporting finer grain sizes of mixed siliciclastic and calcareous or exclusively of calcareous composition. Bed types 5 and 6 are characterized by a siliciclastic matrix with various amounts of siliciclastic and calcareous mud-clasts. They are interpreted as part of a continuous spectrum of beds formed as a consequence of progressive clay enrichment due to entrainment of muddy substrate and that can be classified as transitional flow deposits (*sensu* Baas et al., 2009; 2011; Southern et al., 2016) or hybrid event beds (*sensu* Haughton et al., 2009). Description and interpretation of hybrid event beds was conducted in accordance with the proposed model of Haughton et al. (2009).

Bed type 1.1: Medium- to very thick-bedded, coarse-tail graded microconglomerates

Description: Medium- to very thick-bedded (0.45-5.87 m; mean 1.35 m) microconglomerates. Grain-size ranges from coarse pebbles to fine sand. Beds are characterized by a remarkably poor sorting. The most distinctive textural feature of bed type 1.1 strata is the exclusive presence of coarse-tail grading (Fig. 2.1A). Coarse-tail grading is expressed by a very abrupt fining of the uppermost part of the lowermost microconglomeratic basal division (mean interval thickness ca. 3 – 12 cm), defined by coarse sand matrix-supported granules to medium pebbles that rapidly grade into a weakly graded very coarse to coarse sandstone medial part. The medial part makes up the majority of the bed. The uppermost 5 – 10 cm of individual beds exhibit delayed grading and fine or medium- to fine sandstone. Lateral changes in grain size can be observed as well. Despite faint laminations towards the finer grained tops, beds commonly do not display primary sedimentary structures. Within the medial bed interval, concave-upward water-escape dishes and dewatering sheets are very common (Fig. 2.1B). Only very small proportions of intra-formational rip-up clasts are observed. At the outcrop scale (lateral exposure ca. 15-20 m), beds show good lateral continuity, with bed geometries both tabular and lenticular. Frequent amalgamation depicted by notable grain-size breaks (Fig. 2.1C) result in amalgamated bed-sets up to ca. 23 m thick. Amalgamation contacts locally show erosional relief of up to 20 cm. Bed bases are generally sharp and often ornamented by sole structures (typically groove casts). In the most proximal domain, bed bases locally display loading into underlying finer grained strata and frequently exhibit flame structures

(Fig. 2.1D). Locally, multiple laterally discontinuous traction carpets overlying each other are present, outlined by clast-supported gravelly intervals (thickness 2.5 – 8 cm) that gently fine upward into medium to coarse sand (Fig. 2.1E). They are commonly oriented parallel to bedding or moderately inclined and in rare cases they can be partly deformed (Fig. 2.1E).

Interpretation: Based on the poor sorting, and the internal largely structureless framework, these beds were presumably deposited through rapid fallout from high-density turbidity currents (*sensu* Lowe, 1982; facies show similarity to Lowe S1 and S3 divisions). However, the combination of coarse-tail grading with abundant dewatering structures cannot rule out an alternative interpretation, namely that of a transport by hyperconcentrated to concentrated flows (*sensu* Mulder & Alexander, 2001). The characteristic coarse-tail grading illustrates excessive near-bed sediment concentration (Malgesini et al., 2015), thus supporting the interpretation of a hyperconcentrated- to concentrated density flow origin of the basal interval. The highly concentrated coarse-tail graded lowermost part would suggest traction carpet deposition, whereas the poor to absent grading within the medial parts of beds indicates that deposition most likely occurred by rapid fallout from suspension (“*en masse* deposition” of Lowe, 1982) from rapidly decelerating turbulent flows. Rapid deceleration points to flow expansion (e.g. Jobe et al., 2010; Talling et al., 2012). Coarse-tail graded lowermost parts of beds and locally observed laterally discontinuous traction carpets within the medial parts of beds reflect the complexity of flow characteristics outlined by internal stratification (Sohn, 1997; Janbu et al., 2007). In this case, deposition is related to rapid frictional freezing of a traction carpet following hindered settling through dispersive pressure created by grain-by-grain collisions underneath high-density turbidity currents (Lowe, 1982; Kneller & Branney, 1995). The irregular and deformed nature of some traction carpets might indicate shearing and reworking by internal sediment waves (“pulsing” *sensu* Cartigny et al., 2014), thus pointing towards highly unsteady flow behaviour typified by multiple coarse-grained pulses (c.f. “fluxoturbidites” of Slaczka & Thompson, 1981; see Leszczyński et al., 2015). Delayed normal grading and the presence of traction related sediment structures toward the top of beds suggests progressive grain settling at the waning stages of turbulent flows (Kneller & Branney, 1995), thus supporting the interpretation of turbulent flows with internal stratification. The characteristic presence of coarse-tail grading is suggestive of multiple internal hydraulic jumps within a single event (cf. Postma et al., 1988, 2009). Abundant amalgamations underline a high-energy environment, in which the ratio of amalgamation reflects the time lag between individual subsequent sediment flows and illustrates the erosive nature of the flows (Lien et al., 2006).

Bed type 1.2: Thin-bedded structureless clast-supported microconglomerates

Description: Thin-bedded (0.12-0.45 m; mean 0.30 m), poorly graded, structureless, clast-supported microconglomerates. Intergranular space is filled by a coarse to very coarse sandy matrix containing negligible mud. Grain size ranges from medium sized granules to small pebbles and sorting is moderate to good. Grading is usually poor, although basal inverse grading and relatively abrupt normal grading toward the tops of beds can be observed in some instances. Clasts show a disorganized dispersal pattern and traction or dewatering structures are not observed. Preferred imbrication of clasts is lacking as well. At outcrop-scale (lateral exposure ca. 10-15 m) beds show sheet-like geometries, with sharp basal contacts and flat tops. Sole structures or mud-clasts have not been documented.

Interpretation: The clast-supported texture of these beds suggests that frictional flow was the dominant transport mechanism (Lowe, 1982; Amy & Talling 2007). In particular, negligible presence of clay within the coarse matrix points towards a non-cohesive debris flow, with the good sorting and the scarcity of normal grading implying a hyperconcentrated density flow (grain flow) *sensu* Mulder & Alexander (2001) as being the dominant transport mechanism. Consequently, bed type 1.2 is interpreted to represent basal parts or remnant lags of by-passing high-energy flows (Stevenson et al., 2015) and to be have been deposited from sustained, frictional hyperconcentrated density flows through frictional freezing. Local abrupt normal grading towards the tops of beds is interpreted to illustrate “dumping” or winnowing by overriding, bypassing flows. In addition, the open-framework suggests an effective sorting mechanism that caused extraction of the finer grained fractions, additionally supporting the role of bypass (Stevenson et al., 2015).

Bed Type 1.3: Medium- to thick-bedded inversely graded microconglomerates

Description: Medium- to thick-bedded (0.35-2.45 m; mean 0.85 m), inversely graded microconglomerates. Inverse basal grading is followed by normal grading. Grain size ranges from coarse pebbles (max. 2.1 cm x 4.5 cm) to fine sand, with a poor degree of sorting. Texture is matrix-supported, with a normally graded mud-poor sandstone matrix. While the majority of beds exhibit a range of sedimentary structures, the lowermost parts of beds are typically structureless and only in rare cases display crude cross stratification and clast imbrication. Towards the tops, planar-parallel, wavy- and current-ripple lamination is common. Bed type 1.3 typically have sharp bases. Locally, beds are marked by abrupt grain-size breaks between structureless pebbly lowermost parts and coarse sandy medial parts that display stratifications (Fig. 2.1F). The major proportion of beds show outcrop-scale (lateral exposure ca. 10-15 m) tabular geometries, even if subordinate lenticular geometries occur as well. Tops of beds are sharp and typically flat, only rarely exhibiting an undulating pattern. Loading

structures or sole markings on the bed bases are rare, with only flute casts occasionally present beneath thick beds. Minor amounts of intra-formational rip-up clasts have been observed.

Interpretation: Based on the inversely graded bases followed by normal grading and the presence of primary sedimentary structures, bed type 1.3 is interpreted to have been deposited through tractional fallout from suspension by high- to low-density turbidity currents. Inverse basal grading is interpreted to reflect traction carpet deposition, comparable to the S1 subdivision of Lowe (1982). Abrupt grain-size breaks from pebbles to coarse sand are interpreted to reflect bypass of the granule and very coarse sand fraction down-dip (Stevenson et al., 2015). The presence of crude stratifications and primary sedimentary structures could illustrate the importance of traction processes during deposition or might suggest reworking processes after deposition (Bouma, 1962; Lowe, 1982). Crude stratification is interpreted as being analogous to that characterizing the S3 division of Lowe (1982), whereas the development of wavy- to current ripple-laminations correspond to partial Bouma sequence intervals Tbc deposited under gradually decelerating turbulent flows (Bouma, 1962; Mulder & Alexander, 2001).

Bed type 2.1: Thin- to thick-bedded, graded, structureless sandstones.

Description: Very thin- to thick-bedded (0.07-2.20 m; mean 0.50 m) "clean" sandstones usually showing normal, often delayed grading and a moderate degree of sorting. Locally, beds can exhibit basal inverse grading. Grain size ranges from very coarse to fine sand. Primary sedimentary structures are generally absent, although dewatering structures (dewatering dishes and undulating dewatering sheets) are very common. Only minor proportions (significantly less than 5 % of bed cross section) of intra-formational rip-up clasts are present. At outcrop scale (10s of meters), most beds display tabular geometries, although rare wedge-shaped geometries have been noted. Bases and tops of beds are sharp. Locally, cm-scale groove marks are present at the soles of individual beds.

Interpretation: Because of the delayed normal grading and the absence of primary sedimentary structures, type 2.1 beds are interpreted to have been deposited by fallout from suspension under concentrated density flows or turbulent flows (Mulder & Alexander, 2001). The lack of sedimentary structures reflects rapid deposition, with sediment fallout too fast to be reworked by tractional processes (Lowe, 1982). Dewatering features additionally suggest rapid deposition. The fact that most beds show tabular geometries would suggest that sedimentation occurred rapidly by grain-by-grain deposition due to rapid flow expansion, presumably due to a marked loss in the degree of confinement (Postma et al., 2009; Stow & Johansson, 2000).

Bed type 2.2: Thin- to thick-bedded, graded, structured sandstones

Description: Bed type 2.2 comprises moderately sorted, normally graded thin- to thick-bedded (0.10-1.15 m; mean 0.50 m) fine- to medium “clean” sandstones. In a vertical sequence from their bases toward their tops, beds typically display low-angle planar parallel laminations overlain by wavy and current-ripple laminations. In rare cases, the upper parts of beds show climbing ripples. Locally, beds exhibit dewatering dishes typically associated with small-scale convolute laminations. Bases and tops of beds are sharp and commonly flat. On very rare occasions, small clusters of rip-up clasts can be observed. At the outcrop scale (ca. 15-20 m), beds display both lenticular and tabular bed geometries.

Interpretation: Normal grading, the abundance of primary sedimentary structures and the moderate degree of sorting suggest deposition by fully turbulent flows (Mulder & Alexander, 2001; Crane & Lowe, 2008). With respect to the successive occurrence of laminations, flows can be ascribed to low-density turbidity currents that exhibit partial Bouma sequences. Low-angle planar laminations are interpreted to reflect tractional processes beneath a turbulent flow characterized by upper flow regime conditions (Froude Nr. > 1), corresponding to the Bouma Tb interval. Wavy and current-ripple laminations towards the top of beds indicate late-stage tractional reworking beneath a depleted low-density turbidity current, characterized by deposition under a lower flow regime (Froude Nr. < 1) in unidirectional flows (Bouma Tc interval, see Bouma, 1962; Mulder & Alexander, 2001).

Bed type 3: Heterolithic intervals (clastic and calcareous fine and thin beds)

Description: Heterolithic packages range from 5 cm up to meters thick. Individual beds consist of thin (< 30 cm), graded fine sandstones and calcareous beds intercalated with mudstones and siltstones (Fig. 2.1G). The proportions of individual components can vary considerably. Sandstone beds frequently exhibit wavy- to ripple-laminations. Soles of both sandy and calcareous beds display abundant trace fossils and a clear distinction between ichnofossils assemblages of siliciclastic and calcareous beds can be drawn. Sandstone soles typically feature a trace fossil suite comprising simple, straight and curvilinear non-branching structures such as *Gordia*, *Ophiomorpha* and *Planolites*. On the contrary, branching, meandering and helical trace fossils represented by abundant specimen of *Nereites irregularis* (cf. “*Helminthoides*”; Uchman, 2007), *Thalassinoides*, *Urohelminthoida* and various taxa of the ichnogenus *Chondrites* are developed at the bases of calcareous strata. Bases and tops of the thin sandstone and calcareous beds are sharp, while mudstones and siltstones

intervals can have either sharp or gradational contacts. At the outcrop scale (10s of meters), beds show tabular geometries.

Interpretation: Heterolithic packages are interpreted as resulting from alternating low-energy depositional processes. As denoted by the characteristic normal grading, the fine-grained silty to sandy clastic and calcareous thin beds are interpreted as resulting from suspension fallout of fine-grained tails of diluted turbidity currents. Wavy- and current ripple-laminated fine-grained beds are analogous to Bouma Tc to Td intervals, illustrating traction processes during final waning-flow stages (Mulder & Alexander, 2001). Interbedded muddy intervals are interpreted to represent hemipelagic to pelagic settling, indicating periods of turbidite quiescence (Lien et al., 2006).

Bed type 4: Thin- to thick-bedded calcilutites and calcarenites

Description: Medium- to thick-bedded, graded greyish calcareous sediments (Fig. 2.1H). Grain size ranges from very fine sand (only at the very base of beds) to mud. Beds either have a structureless appearance or, predominantly in the case of the thinner ones, display wavy- to current-ripple laminations towards the bed tops. Soles of beds portray a moderate diversity and high abundance of trace fossils. Comparable to the trace fossils found at the bases of calcareous beds of bed type 3, the observed trace fossil suite corresponds to the typical Helminthoid Flysch trace fossil assemblage. The trace fossil community is dominated by various specimens of the ichnogenera *Helminthoides* (= *Nereites irregularis*; cf. Powichrowski, 1989; Uchman, 2007), *Urohelminthoida* and *Chondrites*. Minor *Orphiomorpha* and *Planolites* traces are also found. Among the peculiarities of bed type 4 is the local presence of sub-horizontal injections of coarse sand within the thick beds (Fig. 2.2A). They are generally lenticular and elongated, with maximum dimensions of up to 0.35 m x 6.50 m. Very rare examples of sub-vertical to vertical injections can also be observed and in some cases they can be traced downwards to their parent sand layer. At the outcrop scale (exposure of up to 100 m), beds appear to be of tabular geometry. Bed bases are generally sharp and flat. Tops are sharp as well, tending to show a wavy shape. Amalgamation of bed type 4 is rare.

Interpretation: Based on the combination of the normal grading and the presence of primary sedimentary structures, bed type 4 is interpreted to record deposition from low-density calcareous turbidity currents. Wavy laminations and ripple-laminations record the effect of traction processes during waning stages of dilute turbulent flows (e.g. Mulder & Alexander, 2001; Felletti, 2016). Localized upward injections of siliciclastic sand from underlying beds are interpreted to reflect the remobilization of the clastic substrate as a result of fluid

overpressure due to gravitational loading (e.g. Andresen & Clausen, 2014; Cobain et al., 2015). Triggering mechanisms for remobilization could include seismic activity, rapid burial or instability of superimposing strata (see Hurst et al., 2011 for review). In the Bordighera Sandstone, with respect to the subduction geodynamic setting (e.g. Di Giulio, 1992), seismicity appears the most likely emplacement trigger.

Bed types 5: Mud-clast enriched sandstone beds

Description: Bed type 5 comprises thin- to thick-bedded microconglomeratic sandstones containing varying proportions of dispersed mud-clasts. Bed thicknesses vary between 17 cm and 2.55 m, with a mean thickness of 1.10 m. Beds are characterized by a general absence of primary sedimentary structures. Locally, dewatering dishes and sheets are present.

Based on the amount and the dominant composition of mud-clasts, two different sub-types (type 5.1 and 5.2) can be distinguished. Bed type 5.1 is defined by roughly equal shares of siliciclastic and calcareous mud-clasts that generally make up less than 10 % of individual beds (Fig. 2.2B). In contrast, bed type 5.2 contains ca. 10-20 % of mud-clasts. In addition, bed type 5.2 mud-clasts are predominantly made up of calcareous substrate, although in some places clusters of scattered siliciclastic mud-flakes are present (Fig. 2.2C). The two sub-types are also defined by textural differences, in particular by the vertical position of mud-clasts within the beds. Bed type 5.1 mud-clasts are usually distributed in the lower part of the beds or immediately above the bed bases. They are commonly aligned parallel to bedding and show minor degrees of deformation. Conversely, mud-clasts of bed type 5.2 are preferably located in the uppermost parts of beds. They are commonly larger than those in bed type 5.1 and locally appear to be disrupted or deformed. Another characteristic feature of bed type 5.2 clasts is the presence of “rims” of dark siliciclastic mud around some of the large calcareous clasts. Additionally, differences in basal grading profiles can be observed. Bed type 5.1 commonly shows normal grading, with the occasional exception of basal inverse grading followed by normal grading. In contrast, bed type 5.2 exclusively exhibits coarse-tail grading.

Both bed types can display thin (< 0.5 cm) horizons of dark siliciclastic mud that can be traced laterally for up to ca. 2.5 m and are characterized by an irregular, wriggling pathway. Bed bases are sharp. Small-scale erosional relief (cm- to dm-scale incisions) occurs locally. Tops are generally sharp as well and they are typically flat, although locally they can be wavy. At the outcrop scale (lateral exposure up to ca. 30 m), bed type 5.1 displays both lenticular and tabular bed geometries, whereas bed type 5.2 strata exclusively exhibit tabular geometries. Observation of lateral passages of bed type 5.1 into bed type 5.2 is rare. Amalgamations of bed type 5 frequently occur, with a maximum number of three amalgamation surfaces being observed within one package. No trends in the vertical arrangement of superimposing bed type 5 varieties is observed.

Interpretation: The common normal grading of bed type 5.1, along with the absence of primary sedimentary structures, point towards high density turbidity currents as being their transport mechanism (Lowe, 1982). The combination of the structureless appearance and normal grading would suggest deposition by fallout from a suspension that prevented tractional processes (S3 division of Lowe, 1982). Mud-clast concentrations illustrate the erosive nature of flows. The occurrence of mud-clasts in clusters prevalently distributed in the lower parts of beds can be interpreted as demonstrating that these clasts were transported along a discrete interface between portions of the flow marked by different densities (cf. Postma et al., 1988). Bed type 5.1 is therewith interpreted as resulting from sediment gravity flows that comprised a turbulent upper part and a lower part showing signs of commencing turbulence dampening (e.g. Sylvester & Lowe, 2004, Southern et al., 2015). Bedding-parallel alignment of mud-clasts suggests that the lower parts of the flows were characterized by incipient turbulence modulation through cohesive mud entrainment (“transitional flow deposits” of Kane & Pontèn, 2012).

Bed type 5.2, showing a combination of a general lack of primary sedimentary structures, coarse grain size and local presence of dewatering structures also appears to have been deposited by high-energy turbulent flows, presumably analogous to the S2 and S3 subdivisions of high-density turbidity currents of Lowe (1982). However, the characteristic presence of coarse-tail grading hints towards a hyperconcentrated flow origin of the basal part (Mulder & Alexander, 2001). The common bedding-parallel orientation of clasts points towards a weakly turbulent flow mechanism that comprises a zone outlined by quasi-laminar flow conditions in which these clasts were dispersed (Stow & Johansson, 2000). High proportions of the muddy components point towards a transition towards more cohesive flow behavior (“plug flow” *sensu* Baas et al., 2009; see Talling et al., 2013). Based on this two-part internal organization, flows are interpreted to be of co-genetic origin, comprising a basal hyperconcentrated density flow overlain by a weakly turbulent flow of high sediment concentration in which enhanced mud entrainment suppressed turbulence (Postma et al., 2009; 2014; Terlaky & Arnott, 2014). High sediment concentration provided the particle-support mechanism for floating mud-clasts (cf. Talling et al., 2013). Bed type 5 might therefore be considered as representing an incipient stage in the development of hybrid event beds *sensu* Haughton et al. (2009).

Bed types 6: Hybrid event beds (HEBs)

Description: Medium- to thick-bedded microconglomeratic sandstones that contain a mud-clast-dominated debritic division. Thicknesses of beds vary between 0.27 m and 3.62 m (average thickness 1.40 m.) Beds are characterized by internal divisions that show very different texture and that are organized in a distinct vertical

sequential order. A poorly sorted, mud-poor basal sandstone interval marked by the absence of traction structures is generally present. Occasionally, small concentrations of mud-clasts and dewatering dishes occur. Basal grain size of the structureless sandstone is up to small pebbles of sub-angular to angular shape. Basal intervals are characterized by the presence of coarse-tail grading followed by poorly developed normal grading. The basal interval is overlain by a disorganized, argillaceous interval enriched in intraformational mud-clasts. Mud-clasts make up at least 20% of the interval, but often they represent a much larger proportion. From a textural perspective, the debritic interval can be described as a matrix-supported mud-clast conglomerate in which clasts are distributed chaotically. The host matrix of the mud-clasts is coarse to very coarse sand and displays delayed normal grading towards the top of the interval. In comparison to the mud-poor sandstone below, it does not exhibit a substantial decrease in grain-size. Mud-clasts are typically angular and have elongated shapes. They primarily consist of calcareous mud. Small amounts of dark siliciclastic mud-clasts and very rare sandstone intra-clasts are also present. Mud-clasts sizes range from cm-scale up to large blocks (average mud-clast size ca. 5 x 15 cm; maximum documented size: ca. 1.75 m x 2.5 m). The sharp contact between the clean sandstone and the debritic division above is usually marked by a thin (cm-scale), laterally continuous wavy horizon of dark siliciclastic mud (except in Bed type 6.3; see below).

Due to their great variability, Bed types 6 strata can be differentiated into three sub-categories (6.1 to 6.3). The main classification criteria is the number of divisions recognized. Bed type 6.1 displays a tri-partite internal makeup that in addition to the two divisions described above comprises a thin (max. ca. 10 cm) mud-poor graded sandstone interval with asymmetric current ripple-laminations that “caps” the debritic division (Fig. 2.2D). On the contrary, bed types 6.2 and 6.3 are defined by their bi-partite internal organization (Fig. 2.2F and 2.2H), with the difference being in the sharp (6.2) or gradational (6.3) character of the divisions boundary.

The character of the chaotic division provides a further substantial criterion for distinction. The color of the muddy coarse sandy matrix of the debritic interval is used as a proxy for mud-content (with a darker matrix being muddier). In bed type 6.1 only the upper part of the debritic division matrix is characterized by a dark color (Fig. 2.2E), while in bed type 6.2 a dark color typically characterizes the entire upper half of the interval and in bed type 6.3 the entire debritic interval is dark (Fig. 2.2H and 2.2I). The dimensions of mud-clasts in bed types 6.1 and 6.2 are generally greater than in bed type 6.3. In some occurrences, bed type 6.2 comprises up to m-scale blocks of preserved and locally undeformed heterolithic stratigraphy (Fig. 2.2F). In bed types 6.1 and 6.2 mud-clasts are distributed chaotically (Figs. 2.2D and 2.2F), whereas bed type 6.3 mud-clasts are more organized, showing a bedding-parallel or quasi-parallel alignment (Fig. 2.2I). The chaotic fabric of bed types 6.1 and 6.2 debritic divisions is often accompanied by a strongly disrupted, folded or sheared nature of the calcareous clasts (Fig. 2.2G). Bed type 6.3 typically comprises isolated clasts that have elongated shapes and do not show strong evidence of deformation.

Basal bed contacts are generally sharp, frequently featuring scouring into underlying sediments. Scours are of m-scale lateral dimensions, with maximum incisional depths of ca. 25 cm. Surfaces of bed tops are commonly flat, occasionally slightly undulating. At the outcrop scale (10s of meters), bed type 6 usually displays tabular geometries. Amalgamation contacts between bed types 6 and bed types 5 are common. In rare cases bed type 6.1 features depositional lateral pinch-outs of the debritic interval (within a few meters), with a transition into bed type 5.

Interpretation:

The characteristic vertical sequential arrangement and varying textural characteristics of bed type 6 divisions demand individual interpretations. Based on the structureless appearance and the poorly graded texture, the mud-poor coarse-tail graded basal divisions are interpreted as deposited by high-concentration frictional flows, analogous to hyperconcentrated density flows of Mulder & Alexander (2001). Sporadic dewatering structures and retarded normal grading entail that these flows were presumably transitional to high-density turbidity currents (sharing strong similarities with the S1-S2 turbidite divisions) *sensu* Lowe (1982). The presence of mud-clasts highlights the erosive nature of these flows, underlining the presence of bedload processes. Deposition is interpreted to have occurred through rapid fallout of the suspended load (Lowe, 1982), with the scarcity of mud throughout the coarse-tail graded interval hinting towards deposition by frictional freezing and successive vertical accretion (Mulder & Alexander, 2001).

The matrix-supported texture of the chaotic division that is dominated by disorganized clasts and elongated blocks of calcareous mud suggests transport by cohesive debris flows defined by the portion of cohesive mud that provides matrix strength as the sediment supporting flow mechanism (Mulder & Alexander, 2001). This interpretation is supported by the presence of either disorganized or broadly bedding-parallel oriented floating clasts and blocks (e.g. Sohn et al., 2002). Angular shapes of mud-clasts indicate limited abrasion (e.g. Hanáček et al., 2013; Cobain et al., 2015) and therewith suggest a relatively short transport distance after entrainment and subsequent rapid collapse of flows (Fonnesu et al., 2016). In particular, the block-dominated nature of bed type 6.2 - in which components of preserved underlying stratigraphy are incorporated into the chaotic subdivision - suggests local mud acquisition and early stages of hybrid flow development (cf. Terlaky & Arnott, 2014; Fonnesu et al., 2016). This interpretation is in accordance with the model proposed by Terlaky & Arnott (2014) that observe clean sandstones containing large rafts made up of preserved internal stratigraphy in a proximal lobe environments and near the axis of flows.

Differences in the amount of mud dispersed within the debritic matrix appear linked to a decrease in mud-clast size and a higher degree of roundness of mud-clasts and are interpreted as related to different stages of the disaggregation of mud-clasts (cf. "starry night" texture of Houghton et al., 2003; Terlaky & Arnott, 2014).

Deposition of the debritic interval is interpreted to have occurred *en masse*, resulting from cohesive freezing as the shear resistance of these flows became balanced with the gravitational force (Mulder & Alexander, 2001). The normal graded mud-poor sandstones displaying current ripple-laminations that “cap” the debritic interval of bed type 6.2 are interpreted as representing the deposit of low-density turbidity currents (Mulder & Alexander, 2001), illustrating deposition and tractional reworking under a dilute tail of the flow that maintained turbulent flow behavior (H4 of Haughton et al., 2009).

Bed type 6 strata are interpreted to record a flow transformation from turbulent to cohesive within one single sedimentation event and therefore can be considered hybrid event beds *sensu* Haughton et al. (2009). With respect to the inferred flow mechanisms of bed type 5 deposits, bed type 6 is interpreted as resulting from more advanced stages of co-genetic flow development during a single sediment gravity flow event (cf. Haughton et al., 2003). The distinction between bed type 5 and bed type 6 is therewith drawn out by the greater proportion of mud-clasts that became incorporated in the coarse sandy matrix. Bed type 6 deposits are interpreted to develop laminar flow development as a result of further increase in clay proportions within the flow compared to bed type 5.

5. Bed type assemblages and their environmental significance

Seven different bed type associations, grouped into three main environmental associations, have been identified in the studied sections of the Bordighera Sandstone. Representative outcrop photographs are shown in Fig. 3 and their main features are summarized in Table 2. Their description and interpretation in terms of depositional environment are discussed in the following section.

Bed type association 1: Channelized associations

Bed type association 1.1: Basin-floor axial feeder channel association

Description: Bed type association 1.1 predominantly consists of “clean” beds types. Mud-poor massive, structureless microconglomerates and medium- to very coarse-grained sandstones represent more than 90 % of bed type proportions. At location 2 (Fig. 1C) this facies association forms a considerably homogenous sandstone body that reaches a thickness of roughly 150 m. Even if lateral dimensions are difficult to constrain due to limited lateral outcrop exposure (Fig. 3A), the exposed large-scale architecture suggests that the width of the sandbody was certainly in the range of at least 1 km or even more. Outcrops accessible for sedimentological logging (ca. 30 m of lateral exposure) reveal both tabular and lenticular geometries at the bed scale. Lenticular bed geometries are observed either in association with incisional contacts of microconglomeratic beds into microconglomerates and sandstones or they occur as scours into heterolithic

intervals. Observed incisional depths are generally small (dm-scale; minimum ca. 10-15 cm). However, local truncations of more than 1 m have been documented (Fig. 3B). Presence of slumped intervals has not been observed. Bed-sets typically encompass clean microconglomerates and sandstones. They are commonly organized in fining-up sequences that internally show high degrees of amalgamation (overall amalgamation ratio: ca. 75 %). Thicknesses of amalgamated intervals vary between ca. 0.8 m and 14.5 m. Within these intervals, a notable feature is the predominance of structureless beds (ca. 65 %) over beds displaying tractional structures. Amalgamated intervals are separated by fine-grained intervals made up of both siliciclastic and calcareous muddy beds, alternating with thin siltstones and fine-grained sandstones beds (0.03-0.25 m thick). The low proportion of muddy intervals results in a considerably high sand-to-mud ratio greater than 10 : 1. Paleocurrent measurements of basal sole structures (groove marks and minor flute casts) reveal unidirectional flows directed toward the North (vector mean = 2°N; n = 14; see Table 2).

Interpretation: The coarse sediment grain size, incisional basal contacts and high amalgamation ratio denote high-energy flow regimes. Dominant proportions of microconglomerates and minor medium- to very coarse-grained "clean" sandstones in association with lenticular bed geometries and internal bed-set organization characterized by fining-upward cycles suggest deposition within a channelized environment (e.g. Champion et al., 2005; Brunt et al., 2013; McHargue et al., 2011, Marchand et al., 2015). A number of observations point towards an axial position within a channel-belt, namely: high portions (75 % of stratigraphic thickness) of amalgamated intervals (e.g. Elliott, 2000; Romans et al., 2009), dominance of structureless sandstones over beds displaying primary sedimentary structures (see Grech et al., 2003) and the scarce presence of beds containing rip-up clasts (Hubbard et al., 2008 and 2014; Macauley & Hubbard, 2013). Small depths of incision for individual events and limited proportions of draping heterolithic packages suggest that the individual channel elements were poorly levee-confined and probably dominated by sheet-like flow processes (Leverenz, 2000). The limited dispersal of paleocurrent orientations suggests a network defined by low-sinuosity channel elements (Hesse et al., 2001; Hubbard et al., 2014). Studies on turbidite systems in trench settings reveal a tendency of unidirectional paleocurrents in channel axes because of large-scale confinement within the trench topography (e.g. Lash, 1985; Underwood et al., 1993). The absence of features recording active slumping processes is interpreted as indicating a low gradient, suggesting the location of the axial channel in a basin-plain setting (Camacho et al., 2002).

Bed type association 1.2: Basin-floor off-axis channel association

Description: Bed type association 1.2 constitute the largest part of section 1 (Fig. 1C). Similarly to Bed type association 1.1, it comprises mainly mud-poor microconglomerates and medium- to very coarse-grained

"clean" sandstones. Clean bed types represent 80-90% of the overall thickness. However, in contrast to BTA 1.1, the relatively thick bed-sets made up of microconglomeratic sandstone beds are in places interrupted by heterolithic intervals consisting of alternating thin-bedded mudstones, siltstones and very fine sandstones (Fig. 3C). Moreover, a decrease in average grain-size in comparison to that of bed type association 1.1 and a reduction in the proportion of basal lag facies can be observed. Among the "clean" bed types, an increase in the portions of beds exhibiting traction structures can be noted, accounting for ca. 40% of microconglomerates and sandstones. In a similar manner to bed type association 1.1, both lenticular and tabular bed geometries are found at outcrop-scale (ca. 10-15 m lateral exposure). Amalgamated bed sets typically exhibit fining-upward trends. The total amalgamation ratio of this bed type association is roughly 60%. Individual thicknesses of amalgamated intervals range from ca. 0.7 m to 6.5 m. Paleocurrent analysis reveals a generally S-N direction (vector mean = 349° N, $n = 14$; circular deviation = $\pm 46^{\circ}$) with a larger variance respect to bed type association 1.1.

Interpretation: The close spatial relationship with bed type association 1.1, the presence of lenticular bed geometries, the rather unidirectional paleocurrent pattern and the fact that bed sets are commonly outlined by fining-upward cycles suggest deposition in a low-sinuosity channelized environment as for BTA 1.1 (e.g. Campion et al., 2005; Satur et al., 2005; McHargue et al., 2011). This bed type assemblage is interpreted to represent a domain located off-axis with respect to bed type association 1.1, based on reduced overall amalgamation ratio (Romans et al., 2009; Rotzien et al., 2014), increased proportions of structured sandstones, more abundant heterolithic intervals (e.g. Camacho et al., 2002; Grecula et al., 2003; Hubbard et al., 2008; McHargue et al., 2011) and slightly finer grain-size (e.g. McHargue et al., 2011; Stanbrook et al., 2015).

Bed type association 1.3: Distributary channel / shallow scour fill association:

Description: Bed type association 1.3 is most abundant at location 7 (Fig. 1C) and it is defined by the dominant presence of highly amalgamated medium- to thick-bedded "clean" microconglomerates and sandstones. It is differentiated from BTA 1.1 and 1.2 mainly on the basis of its location with respect to the overall system extent and on the type of strata found laterally or in stratigraphic contact with it. Bed type association 1.3 has exclusively been observed in the distal domain of the preserved sediment fairway, where it is found intercalated between laterally continuous tabular (outcrop-scale; 10s of meters) strata. Notably, the facies association 1.3 passes laterally or is in direct stratigraphic contact with strata characterized by an increase in mud-enriched bed types and HEBs (bed type association 3; see below).

Sandstones exhibiting physical sedimentary structures such as wavy laminations and current-ripple laminations become more abundant towards the tops of individual bed-sets that display fining-upward trends. Locally,

sandstones enriched in mud-clasts are present as well. Thickness of bed-sets ranges between ca. 2 m and 15 m; with the mean being about 5 m. Well-exposed and laterally continuous outcrops at location 7 allow observation of the lateral extent of bed type association 1.3 intervals approximately orthogonal to paleocurrent orientation. At this location, this facies association is laterally continuous for more than 300-400 meters. Bed type association 1.3 is characterized by (outcrop-scale) slightly lenticular bed-sets, expressed by generally small-scale incisions (below 25 cm) into underlying surfaces. Amalgamated interval thicknesses range from 0.95 m to 4.9 m. The mean vector of paleocurrent measurements is 15° N (circular deviation = $\pm 20^\circ$; n = 4).

Interpretation: Slightly lenticular bed geometries, high degrees of amalgamation within individual bed sets and fining-upward cycles suggest an interpretation as channelized sand bodies. Low incisional depths (dm-scale) and the absence of associated heterolithic strata points towards bed type association 1.3 representing shallow channels of low sinuosity (e.g. Crevello et al., 2007; Rotzien et al., 2014). The absence of lateral passages into heterolithic strata furthermore suggests a lack of levee development (Posamentier & Kolla, 2003; Terlaky et al., 2016). The presence of the bed type association 1.3 in the distal domain of the system, interbedded with laterally continuous, unchannelized strata - attributed to bed type associations 3 - suggests an interpretation as distributary channels associated with intralobe environments (e.g. Brunt et al., 2013; Terlaky & Arnott, 2014). The minor thickness of individual amalgamated elements (compared to BTA 1.1 and 1.2) and the low depth-to-width ratios support this interpretation as distributive channels directly incised into a lobe environment (Saller et al., 2008; Rotzien et al., 2014) recording episodes of progradation of the system (Brunt et al., 2013). An alternative interpretation would be that of bed type association 1.3 representing sandy fills of shallow scours (Hofstra et al., 2015; Pemberton et al., 2016; Terlaky et al., 2016) that likewise would imply sediment bypass.

Bed type association 2: Composite channelized / tabular geometry association

Description: Representative sections (Fig. 1C locations 3 & 4) encompass highly amalgamated, thick-bedded strata comprising both lenticular and tabular beds at the outcrop-scale (max. lateral outcrop exposure ca. 30 m; Fig. 3D). Tabular bed geometries tend to be by far more abundant. Presence of different types of bed geometry is coupled with “mixed” bed type proportions comprising a variety of “clean” (mud-poor) and “dirty” (mud-enriched) bed types. Clean bed types still make up the dominant proportions. In comparison to bed type association 1, an increase in mudclast-rich beds and hybrid event beds occurs at the expense of “clean” bed types. Concerning the portions of fine-grained sediments, siliciclastic muddy and heterolithic bed types account for minor shares of overall thickness. Notably, fine-grained calcareous intervals become more abundant. Infrequent presence of microconglomeratic lags (bed type 1.2) has been observed. However, no clear grain-size

trends within individual bedsets could be identified. A striking feature of bed type association 2 is the repetitive presence of irregular or locally tabular scour surfaces, typically distributed at the bases of thick bed type 5 and 6 strata (Fig. 3E). Scour surfaces are elongated in the direction of the paleoflow and are ornamented by groove marks. Observed depths of incision are in the range of 25-30 cm. Scour dimensions can be in the range of 5 m by 8 m or even greater. Bed type association 2 amalgamation ratios are 65-70 % and amalgamated intervals range in thickness from a minimum of 0.75 m to a maximum of 23.5 m. Bed type association 2 crops out in two adjacent sections (lateral distance of approximately 400 m). Paleocurrent data shows a unimodal mean vector of 308° N (n = 36; see Table 2) characterized by a relatively wide range of dispersal, corresponding to a circular deviation of $\pm 76^\circ$.

Interpretation: The composite presence of both lenticular and tabular beds reflects variable degrees of confinement (see Marini et al., 2015), typically found in a depositional environment typified by a loss in confinement (Brunt et al., 2013). The “mixed” bed type proportions found in this domain of the Bordighera turbidite system can be interpreted as representing sedimentation in the channel-lobe transition zone (*sensu* Mutti & Normark 1987, 1991; cf. Marini et al., 2015). The channel-lobe transition zone is commonly interpreted as marking the shift from confined to unconfined flows (cf. Gardner et al., 2003), expressed through the loss of channel confinement and associated with flow expansion and related enhanced turbulence (Terlaky & Arnott, 2014). Resultant increased erosional capability of the flows is interpreted as being documented by the presence of scours. Scour fields are common not far down-dip of channel mouths (e.g. Wynn et al., 2002; Ito, 2008). Such increased erosional capacity of the flows is also illustrated by the increased proportion of “dirty” bed types on the expense of “clean” microconglomeratic bed types in comparison to elements of bed type association 1 (cf. Fonnesu et al., 2015). The difficulty in correlating two adjacent sections ca. 400 m away from each other (on a transect orthogonal to the main sediment transport) and the presence of punctuated coarse-grained intervals with high sand-to-mud ratios suggest that this depositional interval most probably records rapid avulsions (Bryant et al., 1995; Marsset et al., 2009). As illustrated by the coarse-grained nature of the deposits and the high sandstone-to-mudstone ratio, these avulsions most probably resulted from high sediment supply rates (cf. Milli et al., 2007).

Bed type association 3: Tabular geometry associations

Bed type association 3.1: Axial / proximal lobe association

Description: Bed type association 3.1 is mainly composed of medium to thick beds enriched in mud-clasts (bed types 5), which represent a third of the association (by thickness) and hybrid event beds (bed types 6) which account for a similar share. The remaining portion consists of “clean” sandstones, heterolithic packages and calcareous mud. Although the maximum grain size of coarse-tail graded beds can reach small to medium-sized pebbles, most beds bases include grain sizes up to granules. Some “clean” microconglomerates and “clean” sandstones are also present. Beds show good outcrop-scale lateral continuity (exposures up to 500 m wide), displaying tabular geometry (Fig. 3F). At the bed-set scale, this bed type association is characterized by alternations of coarsening-upwards and fining-upwards trends within intervals denoted by high sand-to-mud ratios. Individual siliciclastic bed-sets are separated by thin intervals of calcareous muddy beds. Noteworthy, the presence of calcareous muddy beds tends to be coupled with an increasing abundance of hybrid event beds. Thicknesses of clastic bed-sets vary between ca. 10 m and 25 m. Internally, bed-sets are denoted by relatively high degrees of amalgamation (mean = 55 %). Amalgamated intervals thicknesses range from 1 m to 8 m. A detailed investigation of the proportions of “dirty” beds (bed types 5 and 6) within amalgamated packages reveals that these make up more than 70% of the amalgamated sands. Paleocurrent measurements of groove casts delineate a rather variable orientation of sediment flux with a circular deviation of $\pm 51^\circ$. Mean paleocurrent dispersal is 35° N (n = 16).

Interpretation: Tabular bedset geometries and alternations of coarsening- and fining-upward cycles suggest a distal realm where beds were deposited by poorly confined flows (e.g. Prélat et al., 2010; Mulder et al., 2010; Brunt et al., 2013). Such bedset-scale trends have been reported from a variety of lobe complexes and they are commonly interpreted to record progradation or lateral shifts of individual lobes and related compensational stacking (e.g. Mutti & Sonnino, 1981; Prélat et al., 2010; Mulder et al., 2010; Grundvåg et al., 2014). The domain characterized by this bed type association is located down-dip (according to the overall paleocurrent trend) of the interpreted channelized domain. This suggests an interpretation as frontal or terminal lobe complexes (*sensu* Morris et al., 2014; cf. Prélat et al., 2010; Mulder & Etienne, 2010). Because of the high degree of amalgamation, the succession can be attributed to the axial zone of a frontal lobe complex (Prélat et al., 2010; Pringle et al., 2010).

Bed type association 3.2: Off-axis lobe association

Description: Bed type association 3.2 is characterized by all the bed types (1-6) accounting for roughly similar shares, with a slight tendency of HEBs being the dominant component of coarse-grained sediments and an abundance of both siliciclastic and calcareous fine-grained sediments. Sand-rich intervals are distinctly

separated by packages of heterolithic strata (ranging from 0.05 m to 2.50 m; overall comprising 13 % of total thickness) and by thin- to thick-bedded fine-grained calcareous beds (bed-sets ranging from 0.10 m to 4 m; representing 16 % of total thickness). In comparison to bed type association 3.1, a significant decrease in sandstone-to-mudstone ratio and bed thickness can be observed. Basal grain size of both clean sandstones and argillaceous sands is up to small pebbles and it is generally finer in comparison to bed type association 3.1. Sand-rich intervals are commonly organized in coarsening-upward cycles followed by fining-upward cycles. Beds display outcrop-scale tabular geometry (up to 500 m lateral exposure; see Fig. 3G). Compared to the axial lobe association (3.1), bed type association 3.2 shows reduced amalgamation ratios (mean = 29 %) and reduced thickness of amalgamated packages (ranging from 0.2 to 5.5 m). Paleocurrent data indicate a mean orientation toward 28° N, with a high variability (circular deviation of $\pm 42^\circ$; $n = 7$).

Interpretation: Tabular bed geometries, together with the high dispersal of paleocurrent directions and the fact that sand-rich units are typically separated by fine-grained intervals, suggest the attribution to an unconfined lobe setting (e.g. Mutti & Normark, 1991; MacDonald et al., 2011; Etienne et al., 2012). The inconsistent stacking pattern within individual bed sets (i.e. both coarsening- and fining-upwards trends) reinforces such interpretation (Prélat & Hodgson, 2013; Terlaky et al., 2016). Based on the reduced degree of amalgamation, reduced grain size and enhanced portions of both fine-grained heterolithic and calcareous intervals, this bed type association can be attributed to the marginal or off-axis lobe realm with respect to the depositional axis of the lobe complex (cf. Prélat et al., 2010; Mulder et al., 2010; Etienne et al., 2012). The typically non-erosive character of the sandy beds is interpreted to reflect the decrease in flow capacity characteristic of distal and marginal lobe environments (e.g. Prélat & Hodgson, 2013; Rotzien et al., 2014).

Bed type association 3.3: Intralobe / lobe fringe association

Description: Bed type association 3.3 is typified by dominant proportions of thin- to very thin-bedded siliciclastic and calcareous bed types. Siliciclastic intervals are made up of alternating thin-bedded mudstones, siltstones and fine to very fine graded sandstones. Calcareous muddy beds account for almost half of the thickness. Fine-grained sandstones and siltstones frequently display current-ripple laminations. Some hybrid event beds are found, but they account for negligible bed type proportions. Microconglomerates and medium- to thick-bedded sandstones are generally absent. Moving further away from amalgamated intervals of BTA 3.1 and 3.2, a notable increase in calcareous bed thickness and proportions and in bioturbation can be observed. Individual beds do not reveal signs of basal erosion and amalgamated intervals are very rare.

Interpretation: The combination of sheet-like bed geometries at the outcrop scale (10s of meters) and the dominance of fine- to very fine-grained heterolithic intervals and muddy calcareous intercalations suggest a

distal lobe environment (e.g. Prélat & Hodgson, 2013; So et al., 2013). With respect to the location within the system, bed type association 3.3 is interpreted to be lateral to the main sediment flux pathways, and can be interpreted as intralobe splay or lobe fringe (Brunt et al., 2013; Terlaky et al., 2016). The increased intensity of bioturbation away from the other bed type associations also supports this interpretation (Heard & Pickering, 2008; Bayet-Goll et al., 2014, 2016).

6 Discussion

6.1 Depositional domains

As shown by the described bed types and their proportions (summarized in Fig. 4), the Bordighera Sandstone can be classified as a coarse-grained, low-efficiency turbidite system (cf. Mutti et al., 1999; Mattern, 2005). It is characterized by high amalgamation ratio and high sand-to-mud ratio that persist down-system (Fig. 4A & 5A). Integration of the sedimentary facies analysis described above with paleocurrent measurements (Fig. 4B) reveals an overall south to north, proximal to distal facies trend. Two main domains can be recognized (logs 1-4 and logs 5-10). The system comprises a relatively proximal channel-belt in the south and extensive terminal splay complexes in the north that extend for more than 30 km of down-dip distance. A striking contrast of dominant bed type proportions along a downstream transect defines a relatively short transition zone that separates the channelized from the lobate associations (Figs. 5B and 6A).

The proximal domain is defined by the presence of channelized bed type associations characterized by highly amalgamated (up to 75 %) and thick (up to 15 m) intervals dominated by mud-poor bed types (1 and 2). High sand-to-mud ratios range from 11:1 to 4:1 (axis to off-axis). The axial channel realm (e.g., log 2, Fig. 4) is made up by microconglomerates (82 %) and sandstones (12 %). Heterolithic intervals (3 %) and calcareous muddy intercalations (ca. 2%) are very rare. Mudclast-rich beds and HEBs (combined ca. 1 %) are negligible. From an hydrocarbon reservoir point of view, these deposits should result in very high vertical and lateral connectivity, as migration barriers are almost absent (cf. Brunt & McCaffrey, 2007).

The off-axis channel realm (e.g., log 1, ca. 8 km across-current from log 2; Fig. 4), exhibits an increase in the proportions of clean sandstones (18 %) at the expense of microconglomeratic beds (69 %). Heterolithic intervals portions remain low (3 %), and only a moderate increase in calcareous beds (5 %), mudclast-rich beds (4 %) and HEBs (1 %) is documented. With respect to the overall S-N facies trend, the channelized domain is interpreted to represent the feeder channels that supplied depositional lobes further basin-wards (e.g. Wynn et al., 2002; Terlaky et al., 2015). As sandbody heterogeneities related to clay entrainment and levee

development are negligible, the off-axis channel association similarly represents a component of the system marked by high vertical and lateral connectivity (cf. Brunt & McCaffrey, 2007).

The transitional zone between the channelized and the lobate domain is of limited basin-ward extent (c. 5-7 km; Fig. 5B; see also Fig. 4, logs 3 & 4), making up only 1/10 of the preserved system (Fig. 6A). The bed type association (composite channelized / tabular) is characterized by high amalgamation ratios (65-70 %) and a mean sand-to-mud ratio of 6:1. Then two investigated sections are in close lateral vicinity (300-400 m distance orthogonal to paleoflow) and are characterized by frequent shifts regarding the stratigraphic distribution of very coarse grained intervals (see highlighted box in Fig. 6B). This is interpreted to reflect rapid avulsion due to high sedimentation rates (cf. Bryant et al., 1995). Maximum thickness of individual amalgamated intervals is the greatest in the system (up to 24 m). Notably, an increase in mud-rich beds (mud-clast rich beds: 10 %; HEBs: 7 %) at the expense of clean bed types (microconglomerates: 57 %, sandstones: 15 %) is observed. Heterolithic intervals (3 %) remain relatively low, whereas calcareous muddy beds (11 %) considerably increase. A more gradual transition from a proximal zone to an extensive medial domain and then to a distal submarine fan association typical of some basin plain submarine fans (e.g. Mattern, 2005) is not developed. High degrees of amalgamation and high sandstone-to-mudstone ratios are contrasted by both the emergence of sandstones rich in mud-clasts and the enhanced presence of muddy beds that would constitute flow barriers and therefore reduce reservoir volume and connectivity (cf. Brunt & McCaffrey, 2007).

The relatively short transitional domain is replaced by a lobe domain dominated by mud-clast-enriched sandstone beds and HEBs. The axial lobe bed type association (e.g., section 6; Fig. 4) shows high amalgamation rates (> 55 %) and related high sand-to-mud ratio (5.5 : 1). Maximum thickness of amalgamated intervals is ca. 15 m. While mud-rich beds are dominant (mud-clast enriched beds: 30 %; HEBs: 33 %) and clean bed type proportions are starkly reduced (microconglomerates: 17 %; sandstone: 9 %), the proportions of heterolithic intervals (2 %) and calcareous intercalations (9 %) do not record significant changes in abundance. On the contrary, the off-axis lobe association (e.g., section 5; Fig. 4) is characterized by a lesser degree of amalgamation (15 %) and related sand-to-mud ratio (1.5 : 1). This is coupled with thinner bed-sets and a further decline in coarse clean bed type proportions (microconglomerates: 12 %), which is partly compensated by sandstones increase (15 %), but also, with respect to the axial lobe environment, with a smaller amount of mud-clast enriched beds and HEBs (16% and 28 % of stratigraphic thickness respectively). Furthermore, fine-grained bed type proportions increase (heterolithic intervals: 13 %; calcareous intercalations: 16 %). Albeit defined by high degrees of amalgamation and high sand-to-mud ratios, the impact of the mud-rich sandstones within the amalgamated intervals is interpreted to result in barriers to fluid flow (cf. Brunt & McCaffrey, 2007).

Finally, the marginal distal association (sections 8-10; Fig. 4) records the progressive pinch-out of the siliciclastic succession. It is defined by low degrees of amalgamation (5 %), low sand-to-mud ratio and a substantial decrease in clean bed types (microconglomerates: <5 %; sandstones: ca. 10 %). The occurrence of mud-clast enriched beds (ca. 15 %) and HEBs (ca. 10 %), is coupled with abundant heterolithic and calcareous intervals (ca. 30 % each). The distributive channel association is only present in the distal domain (section 7, Fig. 4) and it is marked by high amalgamation rates (ca. 85 %), high sand-to-mud ratio (9 : 1), high proportions of clean bed types (ca. 75 % microconglomerates, ca. 20 % sandstones), minor amounts of heterolithic intervals (ca. 5 %), along with the absence of mud-rich bed types and HEBs. This facies association occurs in intervals of limited vertical thicknesses (2- 15 m; mean: ca. 5 m) and lateral extent (ca. 300-400 m estimated) and it is therewith interpreted to constitute only a limited portion of the stratigraphy in the distal domain.

6.2 Mud-rich sandstones

Observed bed type distributions provide the basis for idealized trends of cross-current (Fig. 7A-B) and down-current stacking pattern motifs (Fig. 7C). These stacking pattern motifs outline the relatively homogeneous vertical and lateral character of the channel-fill association in contrast with the more heterogeneous character (both vertically and laterally) of the unconfined domain, characterized by mudclast-rich beds and by hybrid event beds (HEBs). This onset of mud-rich sandstones occurring in the transitional domain is associated with an increase in the presence of calcareous mud intervals (see Fig. 5B), which constitute the material that is commonly found incorporated in the mud-rich sandstones as mudclasts. This observation suggests that a combination of the erosive nature of the flows and the availability of cohesive calcareous substrate might have promoted HEB development.

Close resemblances between the mudclast-rich sandstone beds of the Bordighera and the matrix-rich sandstones described by Terlaky & Arnott (2014) can be noted. On the one hand, the generally coarse grain size of beds is similar. On the other hand, essentially in the case of bed type 5.2, the coarse-tail graded nature and the corresponding bi-partite internal organization of beds represent striking similarities to the type 4 matrix- rich sandstones of the Kaza Group. Furthermore, the internal texture of mudclasts, marked by angular shapes is analogous to the shape of mudclasts described by Terlaky & Arnott (2014). Typically angular shaped clayey clasts and rafts illustrate erosion of a comparably proximal source of muddy material rather than further up-dip acquisition of muddy substrate (e.g. Terlaky & Arnott, 2014; Fonesu et al., 2016). In terms of flow processes, both the Bordighera mudclast-rich beds and the matrix-rich strata of Terlaky & Arnott (2014) have the hyperconcentrated density flow origin of the basal clean sandstone in common.

The hybrid event beds in the Bordighera system are characterized by a debritic division (H3 of Haughton et al., 2009) made up of an argillaceous coarse sandstone packed with calcareous mudclasts. In this respect, they are very different from the finer grained transitional flow deposits of Kane & Pontén (2012) and Southern et al. (2016). As for mudclast-rich beds, the typically angular shape of the mudclasts suggest that mud acquisition occurred within a limited basin-ward distance. This is in agreement with Fonnesu et al. (2016), who proposed the local delamination of blocks of underlying substrate as triggering progressive HEB emergence. In the Bordighera case, such tendency of local mud incorporation is both reflected by the mud-poor textural character of the bed types that define the feeder channel association and the sudden appearance of beds enriched in mudclasts in the realm defined by a loss of channel confinement. Progressive stages of mudclasts disaggregation subsequent to local substrate entrainment are reflected by increasing thicknesses of the portions of the matrix of debritic intervals displaying a very muddy "starry night" appearance.

Spatial distribution of HEB types (Fig. 8A) shows that proportions of bed types 6.2 and 6.3 deposits tend to become greater towards the distal axial lobe domain. Analysis of the ratio of the debritic division thickness to full bed thickness of bed type 6 sub-types (Fig. 8B) indicates a progressive increase in the proportion of the debritic H3 division from types 6.1 to 6.3. The combination of these two observations illustrate the occurrence of a systematic basin-ward trend of beds becoming increasingly enriched in muddy substrate.

The observed spatial distribution of hybrid event beds - in particular their abundance in the interpreted axial lobe domain - partly contrasts with published models on their occurrence in turbidite systems. The bulk of existing models places hybrid event beds in distal and lateral fan environments, particularly in fan-fringes (e.g. Haughton et al., 2009; Hodgson et al., 2009; Southern et al., 2016; Sychala et al., 2017). More proximal occurrence of HEB development has been attributed to up-section backfilling of proximal channels (Haughton et al., 2009) as well as to rapid deceleration of sediment gravity flows in response to onlapping relationships with confining topography (Patacci et al., 2014). Conversely, the distribution of mudclast-rich sandstones and hybrid event beds in the Bordighera turbidite system appears to reveal a different scenario, namely that of their emergence in close down-dip proximity to the channel lobe transition zone. Terlaky & Arnott (2014) document a similar onset for argillaceous sandstones in the proximal basin-floor environment. The authors interpret the rapid occurrence of stacked depositional lobes as the result of avulsion at the termination of channelized structures. Resulting supercritical flows ("unconfined jet flows") are interpreted to have entered the mud-dominated unconfined basin-floor and enhanced erosional capability promoted the incorporation of substrate and subsequent transitional flow behavior. In addition, existing models (e.g. Haughton et al., 2009; Fonnesu et al., 2015; Southern et al., 2015) assign the spatial expansion of HEB prone associations to relatively limited down-dip distances. On the contrary, in the Bordighera turbidite system the hybrid-prone interval

stretches for at least 30 km down-dip. The very high-energy and coarse-grained nature of the system, coupled with the presence of cohesive calcareous substrate might be able to explain such differences, although further work is required to establish a process model for how this might occur.

7 Conclusions

- The coarse-grained Bordighera turbidite system is characterized by high sand-to-mud ratio throughout the sediment pathway, revealing the capacity of the system in supplying coarse fractions to the very distal realms.
- The down-dip transition (of limited spatial extent) from a channelized proximal setting into an extensive sheet association is coupled with an increase in calcareous intervals and with the emergence of abundant mudclast-rich sandstones and hybrid event beds.
- The abundance of coarse-grained mudclast-rich sandstones and hybrid event beds in the high-energy axial proximal lobe environments marked by high sandstone to mudstone ratio has been reported only in a limited number of systems and it might be characteristic to the Bordighera because of the availability of cohesive calcareous mud.
- The average thickness of amalgamated intervals does not decrease significantly throughout the observed part of the system. Notwithstanding, promising high hydrocarbon reservoir quality because of the high sand-to-mud ratio is impaired by the fact that internal connectivity might be affected by bed-scale heterogeneity due to the abundance of mudclast-rich beds and hybrid event beds.

Acknowledgements

Financial support for this research was provided by the University of Pavia PhD research grant of Pierre Mueller and by the Turbidites Research Group sponsors: Anadarko, BG Group, BP, ConocoPhillips, Dana Petroleum, ENI, Nexen, OMV, Petronas, Shell, Statoil and Woodside. The Orengo family is warmly acknowledged for their kind hospitality in providing accommodation in Badalucco during fieldwork. We are deeply indebted to reviewers Salvatore Milli and Viktor Terlaky whose detailed and constructive comments helped to significantly improve the manuscript. Journal editor Thomas Hadlari is thanked for the handling of the manuscript and valuable suggestions that enhanced the clarity of the text.

Figure Captions

Fig. 1: (A & B) Location of the study area. (C) Geological map illustrating location of measured sections (1-10). (D) Chronostratigraphic framework of the San Remo Unit. Modified from Lanteaume (1990), Di Giulio (1992) and Maino et al., 2012; 2015.

Fig. 2.1: Outcrop examples of selected bed types (1-4). (A) Coarse-tail graded pebbly base of bed type 1.1; the bed is overturned and the field of view shows the basal surface of the bed. Note the angular shape of basal pebbles (arrow); section 2, Badalucco-Quarry. (B) Dewatering dishes in bed type 2.1 strata; section 4, "Montalto River". (C) Amalgamations (arrows) between bed type 1.1 microconglomerates in the axial proximal realm; outcrop close to "Ospedaletti". (D) Basal loading of bed type 1.1 into underlying finer-grained strata. Note deformed base with flame structures (arrows). Outcrop close to "Ospedaletti". (E) Slightly deformed traction carpets superimposing coarse-tail graded base of bed type 1.1; section 2, Badalucco-Quarry. (F) Bed type 1.3 displaying typical vertical arrangement of a pebbly structureless base overlain by a coarse sandy medial part with cross-stratifications, followed by weakly inclined cross-lamination and wavy- to ripple-laminated toward the top of the bed. Note the abrupt grain-size jump between the basal and middle divisions. Section 4, "Montalto River". (G) Heterolithic interval characterized by alternating calcareous and siliciclastic fine-grained thin beds; section 5, "Carmo dei Brocchi". (H) Alternating medium- to thick-bedded calcareous beds; section 6, "Monte Frontè".

Figure 2.2: Outcrop examples of selected bed types (4-6). (A) Sill-like clastic sand injection into thick-bedded calcareous mud (Bed type 4); section 8 "Margheri Binda". (B) Bedding-parallel "floating" calcareous clast (arrow) incorporated into bed type 5.1 strata; section 5, "Carmo dei Brocchi". (C) Cluster of calcareous and siliciclastic mud clasts (yellow arrows) within bed type 5.2. Note the broadly bedding-parallel alignment of the smaller clasts (white arrows). Section 6 "Monte Frontè". (D) Tri-partite hybrid event bed characterized by strongly disrupted and folded calcareous clasts. Yellow line indicates the base of the bed. Note the thin capping H4 division; section 6 "Monte Frontè". (E) Detail of upper part of bed shown in (D): laminated H4 division superimposing the debritic H3 division. Note the dark colour of the matrix of the H3 division indicating clay dispersed into the uppermost part of the coarse sandstone matrix and the down-ward injection of H4 clean sand into the H3 interval (arrow). (F) Bi-partite hybrid event bed (bed type 6.1) containing a block of preserved heterolithic stratigraphy incorporated in the H3 division (red arrow). Note strongly deformed large calcareous mud-clasts above the block. Section 6 "Monte Frontè". (G) Detail of mud-clast deformation of bed shown in (F). (H) Example of bed type 6.3, characterized by gradational HEB divisions. Note the roughly bed-parallel

calcareous clasts and blocks making most of the H3 division and the thin H1 interval. Section 10 “Cima di Velega”. (I) Detail of bed type 6.3, showing roughly bed-parallel clasts and very dark sandy matrix.

Fig. 3: Bed type associations. (A) Sandbody geometry showing high sand content in the interpreted channel axis (bed type association 1). Lateral onlap of bed-sets is interpreted to demonstrate erosional character of the channel. View towards N-NW. Exposure cropping out on the opposite side of the valley of “Badalucco-Quarry” (Section 2). (B) Incisional bases truncating into finer-grained strata characteristic of the axial channelized association. Section 2 “Quarry Badalucco”. (C) Heterolithic intervals typifying bed type association 1.2. Section 1 “Monte Bignone”. (D) Composite tabular and lenticular bed geometries characterizing bed type association 2. Note the predominance of tabular bed geometries and the high sand-to-mud ratio. Section 4 “Montalto River”. (E) Detail of tabular scour surface at the base of overturned thick mudclast-rich bed (bed type association 2). Yellow arrows indicate the orientations of groove casts ornamenting the scour surface. Mean paleocurrent direction is towards the NNW. Section 4 “Montalto River”. (F) Example of bed type association 3.1 cropping out in an anticlinal structure. Note the sheet-like geometry and high sand-to-mud ratio. Section 6 “Monte Frontè”. (G) Bed type association 3.2 characterized by sheet-like geometry and by a reduced sand content in comparison to bed type association 3.1. Section 9 “Monte Bertrand”.

Fig. 4: (A) Dataset for the 10 studied sections. For each section, from left to right: i) bar indicating amalgamated intervals (green); ii) bar indicating bed type associations; iii) synthetic log showing bed thickness, grain size and bed type (colors); iv) vertical bed type proportions (continuous running average over a window of 10 meters). (B) Map of the log locations with paleocurrent measurements.

Fig. 5: (A) Amalgamation ratios for the ten measured sections (numbers; see Fig. 1C) ordered from proximal to distal. Lower percentages of amalgamations are interpreted to indicate locations off-axis to marginal with respect to the axis of the sediment fairway. (B) Relative proportions of clean bed types (bed types 1 & 2), mud-rich bed types (bed types 5 & 6) and muddy strata (bed types 3 & 4) along a proximal to distal transect. Distances between sections have been calculated on the basis of their inferred depositional position after structural restoration. Numbers indicate section number; see Fig. 1C.

Fig. 6: Inferred gross geometry of the Bordighera Sandstone. (A) Inferred extension of channelized associations, composite (i.e. transitional) associations and lobe associations. (B) Vertical synthetic grain size profiles for measured logs (continuous running average over a window of 10 meters). Note the presence of very coarse fractions in the distal domain. The red box highlights logs 3 and 4 (300-400 m distance orthogonal to paleoflow) where very coarse grained intervals cannot be correlated, suggesting an environment characterized by rapid avulsions.

Fig. 7: Idealized stacking pattern motifs: (A) axial channel to off-axis channel; (B) axial lobe to off-axis lobe and (C) proximal to distal. Distances correspond to restored depositional positions of outcrops.

Fig. 8: (A) HEB types proportions in different depositional domains. (A) Ratio of debritic interval thickness to full bed thickness of hybrid event bed types.

Table captions

Table1: Summary of bed type descriptions and interpretations.

Table 2: Summary of bed type associations descriptions and interpretations.

References

- Amy, L.A. & Talling, P.J. (2008). Basin-plain deposits of the Marnoso Arenacea Formation, Italy. In: Nilsen, T.H., Shew, R.D., Steffens, G.S., Studlick, J.R.J. (Eds). *Atlas of Deep-Water Outcrops*. AAPG Studies in Geology, 56, 215-217.
- Amy, L.A., Peachey, S.A., Gardiner, A.A., Talling, P.J. (2009). Prediction of hydrocarbon recovery from turbidite sandstones with linked-debrite facies: Numerical flow-simulation studies. *Marine and Petroleum Geology*, 26, 2032-2043.
- Andresen, K.J. & Clausen, O.R. (2014). An integrated subsurface analysis of clastic remobilization and injection; a case study from the Oligocene succession of the eastern North Sea. *Basin Research*, 26 (5), 641-674.
- Baas J.H., Best J.L., Peakall J., Wang M. (2009). A phase diagram for turbulent, transitional, and laminar clay suspension flows. *Journal of Sedimentary Research*, v. 79, p. 162–183
- Baas, J.H., Best, J.L., Peakall, J. (2011). Depositional processes, bedform development and hybrid bed formation in rapidly decelerated cohesive (mud-sand) sediment flows. *Sedimentology*, 58, 1953-1987.
- Barker, S. P., Haughton, P. D. W., McCaffrey, W. D., Archer, S. G. and Hakes, B. (2008). Development of rheological heterogeneity in clay-rich high-density turbidity currents: Aptian Britannia Sandstone Member, UK continental shelf. *Journal of Sedimentary Research* 78(1-2): 45-68.
- Bayet-Goll, A., Neto de Carvalho, C., Moussavi-Harami, R., Mahboubi, A., Nasiri, Y. (2014). Depositional environments and ichnology of the deep-marine succession of the Amiran Formation (Upper Maastrichtian-Paleocene), Lurestan Province, Zagros Fold-Thrust Belt, Iran. *Palaeogeography, Palaeoclimatology, Palaeoecology*, 401, 13-42.
- Bayet-Goll, A., Monaco, P., Jalili, F., Mahmudie-Gharaie, M.-H. (2016). Depositional environments and ichnology of Upper Cretaceous deep-marine deposits in the Sistan Suture Zone, Birjand, Eastern Iran. *Cretaceous Research*, 60, 28-51.
- Bouma, A. (1962). *Sedimentology of Some Flysch Deposits: a Graphic Approach to Facies Interpretation*. Elsevier, New York.

Brunt, R.L. & McCaffrey, W.D. (2007). Heterogeneity of fill within an incised channel: The Oligocene Grès du Champsaur, SE France. *Marine and Petroleum Geology*, 24, 529-539.

Brunt R.L., Hodgson D.M., Flint S.S., Pringle, J.K., Di Celma C., Prélat A. & Grecula M. (2013). Confined to unconfined: Anatomy of a base of slope succession, Karoo Basin, South Africa. *Marine and Petroleum Geology*, 41, 206-221.

Bryant, M., Falk, P., Paola, C. (1995). Experimental study of avulsion frequency and rate of deposition. *Geology*, 23 (4), 365–368.

Camacho, H., Busby Spera, C. J., Kneller, B. C. (2002). A new depositional model for the classical turbidite locality at San Clemente State Beach, California. *AAPG Bulletin*, 86 (9), 1543-1560.

Campion, K. M., Sprague, A.R.G., Sullivan, M. D. (2005). Architecture and lithofacies of the Capistrano formation (Miocene-Pliocene), San Clemente, California. *The Pacific Section SEPM*, 42 p.

Cartigny, M.J.B., Ventra, D., Postma, G., Van den Berg, J.H., (2014). Morphodynamics and sedimentary structures of bedforms under supercritical-flow conditions: New insights from flume experiments. *Sedimentology*, 61 (3), 712-748.

Cobain, S.L., Peakall, J., Hodgson, D.M. (2015). Indicators of propagation direction and relative depth in clastic injectites: implications for laminar versus turbulent flow processes. *Geological Society of America Bulletin*, 127, 1816–1830.

Cobianchi M., Di Giulio A., Galbiati B., Mosna, S. (1991). Il “complesso di base” del Flysch di S. Remo nell’area di S. Bartolomeo, Liguria occidentale (nota preliminare). *Atti Ticinesi Scienze della Terra*, 34, 145–154.

Crane, W.H. & Lowe, D.R. (2008). Architecture and evolution of the Paine channel complex, Cerro Toro formation (Upper Cretaceous), Silla syncline, Magallanes basin, Chile. *Sedimentology*, 55, 979-1009.

Crevello, P. D., H. D. Johnson, F. Tongkul, Wells, M. R. (2007). Mixed braided and leveed-channel turbidites, West Crocker fan system, northwest Borneo. *In*: T. H. Nilsen, R. D. Shew, G. S. Steffens, and J. R. J. Studlick, *AAPG Deep-water Atlas*.

Davis, C., Houghton, P.D.W., McCaffrey, W.D., Scott, E., Hogg, N., Kitching, D. (2009) Character and distribution of hybrid sediment gravity flow deposits from the outer Forties Fan, Palaeocene Central North Sea, UKCS. *Marine and Petroleum Geology*, 26, 1919-1939.

Decarlis, A., Dallagiovanna, G., Lualdi, M., Maino, M., Seno, S. (2013). Stratigraphic evolution in the Ligurian Alps between Variscan heritages and the Alpine Tethys opening: A review. *Earth-Science Reviews*, 125, 43–68.

Di Giulio, A. (1992). The evolution of the Western Ligurian Flysch Units and the role of mud diapirism in ancient accretionary prisms (Maritime Alps, Northwestern Italy). *Geologische Rundschau*, 81, 655-668.

Elliott, T. (2000). Depositional architecture of a sand-rich, channelized turbidite system: The Upper Carboniferous Ross Sandstone Formation, Western Ireland: GCSSEPM Foundation 20th Annual Research Conference Deep-Water Reservoirs of the World, 342-373.

Etienne, S., Mulder, T., Bez, M., G. Desaubliaux, G., Kwasniewski, A., Parize, O. Dujoncquoy, E., Salles, T. (2012).

Multiple scale characterization of sand-rich distal lobe deposit variability: Examples from the Annot Sandstones Formation, Eocene–Oligocene, SE France. *Sedimentary Geology*, 273–274, 1-18.

Felletti, F. (2016). Depositional architecture of a confined, sand-rich submarine system: the Bric la Croce-Castelnuovo turbidite system (Tertiary Piedmont Basin, Oligocene, NW Italy) *Ital. J. Geosci.*, 135 (3), 365-382.

Fonnesu, M., Haughton, P., Felletti, F., McCaffrey, W.D. (2015). Short length-scale variability of hybrid event beds and its applied significance. *Marine and Petroleum Geology*, 67, 583-603.

Fonnesu, M., Patacci, M., Haughton, P.D.W., Felletti, F., McCaffrey, W.D. (2016). Hybrid Event Beds Generated By Local Substrate Delamination On A Confined-Basin Floor. *Journal of Sedimentary Research*, 86 (8), 929-943.

Fonnesu, M., Felletti, F., Haughton, P.D.W., Patacci, M., McCaffrey, W.D. (2017). Hybrid event bed character and distribution linked to turbidite system sub-environments: the North Apennine Gottero Sandstone (north-west Italy). *Sedimentology*, doi: 10.1111/sed.12376

Galbiati B. & Cobianchi, M. (1997). L'indipendenza tettonica dell'unità di Sanremo rispetto all'unità di Moglio-Testico. *Bollettino Societa Geologica Italiana*, 116, 453–472.

Gardner, M.H., Borer, J.M., Melick, J.J., Mavilla, N., Dechesne, M., Wagerle, R.N. (2003). Stratigraphic process-response model for submarine channels and related features from studies of Permian Brushy Canyon outcrops, West Texas. *Marine and Petroleum Geology*, 20, 757–787.

Giammarino, S., Fanucci, F., Orezzi, S., Rosti, D., & Morelli, D. (2010). Foglio 258–271 San Remo. Note illustrative della carta geologica d'Italia alla scala 1:50.000. Roma: Servizio Geologico d'Italia.

Grech, M., Flint, S. S., Wickens, H. d. V., Johnson, S. D. (2003). Upward-thickening patterns and lateral continuity of Permian sand-rich turbidite channel fills, Laingsburg Karoo, South Africa. *Sedimentology*, 50, 831-853.

Grundvåg, S.A., Johannessen, E.P., Helland-Hansen, W., Plink-Björklund, P. (2014). Depositional architecture and evolution of progradationally stacked lobe complexes in the Eocene Central Basin of Spitsbergen. *Sedimentology*, 61, 535-569.

Haughton, P.D.W., Barker, S.P., McCaffrey, W.D. (2003). 'Linked' debrites in sand-rich turbidite systems - origin and significance. *Sedimentology*, 50, 459-482.

Haughton, P.D.W., Davis, C., McCaffrey, W.D., Barker, S. (2009). Hybrid sediment gravity flow deposits - Classification, origin and significance. *Marine and Petroleum Geology*, 26, 1900-1918.

Heard, T.G. & Pickering, K.T. (2008). Trace fossils as diagnostic indicators of deep-marine environments, Middle Eocene Ainsa-Jaca Basin, Spanish Pyrenees. *Sedimentology*, 55, 809-844.

Henstra, G.A., Grundvåg, S.-A., Johannessen, E.P., Kristensen, T.B., Midtkandal, I., Nystuen, J.P., Rotevatn, A., Surlyk, F., Sæther, T., Windelstad, J. (2016). Depositional processes and stratigraphic architecture within a coarse-grained rift-margin turbidite system: the Wollaston Forland Group, east Greenland. *Marine and Petroleum Geology*, 76, 187–209.

- Hanáček, M., Daniel Nývlt, D., Flašar, J., Stacke, V., Mida, P., Lehejček, J., Tóthová, G., Břežný, M., Procházková, B., Uxa, T., Křenovská, I. (2013). New methods to reconstruct clast transport history in different glacial sedimentary environments: Case study for Old Red sandstone clasts from polythermal Hørbyebreen and Bertilbreen valley glaciers, Central Svalbard. *Czech Polar Reports*, 3 (2), 107-129.
- Hesse, R., Klauke, I., Khodabakhsh, S., Piper, D.J.W., Ryan, W.B.F., NAMOC Study Group (2001). Sandy submarine braid plains: Potential deep-water reservoirs. *AAPG Bulletin*, 85, 1499–1521
- Hodgson, D.M. (2009). Distribution and origin of hybrid beds in sand-rich submarine fans of the Tanqua depocentre, Karoo Basin, South Africa. *Marine and Petroleum Geology*, 26 (10): 1940-1956.
- Hofstra, M., Hodgson, D.M., Peakall, J., Flint, S.S. (2015). Giant scour-fills in ancient channel-lobe transition zones: Formative processes and depositional architecture: *Sedimentary Geology*, 329, 98–114.
- Hubbard, S.M., Romans, B.W., Graham, S.A. (2008). Deep-water foreland basin deposits of the Cerro Toro Formation, Magallanes basin, Chile: architectural elements of a sinuous basin axial channel belt. *Sedimentology*, 55, 1333-1359.
- Hubbard, S.M., Covault, J.A., Fildani, A., Romans, B.W. (2014). Sediment transfer and deposition in slope channels: deciphering the record of enigmatic deep-sea processes from outcrop. *GSA Bulletin* 126, 857–871.
- Hurst, A., Scott, A., Vigorito, M. (2011). Physical characteristics of sand injectites: *Earth-Science Reviews*, 106, 215–246.
- Hurst, A., Scott, A., Vigorito, M. (2011). Physical characteristics of sand injectites. *Earth-Science Reviews*, 106, 215–46.
- Ito, M. (2008). Downfan transformation from turbidity currents to debris flows at a channel-to-lobe transitional zone; the lower Pleistocene Otadai Formation, Boso Peninsula, Japan. *Journal of Sedimentary Research*, 78 (10): 668-682.
- Janbu, N. E., Nemeč, W., Kirman, E., Ozaksoy, V. (2007). Facies anatomy of a sand-rich channelized turbiditic system: the Eocene Kusuri Formation in the Sinop Basin, north-central Turkey. In: Nichols, G., Williams, E. and Paola, C. (Eds). *Sedimentary Processes, Environments and Basins: A Tribute to Peter Friend*. Special Publications of the International Association of Sedimentologists, 38, 457-517.
- Jobe, Z.R., Bernhardt, A., Lowe, D.R. (2010). Facies and architectural asymmetry in a conglomerate-rich submarine channel fill, Cerro Toro Formation, Sierra Del Toro, Magallanes Basin, Chile. *Journal of Sedimentary Research*, 80, 1085-1108.
- Kane, I.A. & Pontén, A.S.M. (2012). Submarine transitional flow deposits in the Paleogene Gulf of Mexico. *Geology*, 40, 1119-1122.
- Kneller, B.C. & Branney, M.J. (1995). Sustained high-density turbidity currents and the deposition of thick massive sands. *Sedimentology*, 42, 607-616.
- Lanteaume, M., Radulescu, N., Gavos, M., & Feraud, J. (1990). Notice explicative, Carte Géol. De France (1/50.000), feuille Viève-Tende (948). Orleans: BRGM. 139 pp.
- Lash, G.G. (1985). Recognition of trench fill in orogenic flysch sequences. *Geology*, 13, 867-870.

Leszczyński, S., Dziadzio, P.S., Nemeč, W. (2015). Some current sedimentological controversies in the Polish Carpathian flysch. Guide to field trip B8, 31st IAS Meeting of Sedimentology Kraków, Poland, 25–27 June.

Leverenz, A. (2000). Trench-sedimentation versus accreted submarine fan; an approach to regional-scale facies analysis in a Mesozoic accretionary complex; "Torlesse" Terrane, northeastern North Island, New Zealand. *Sedimentary Geology*, 132(1-2), 125-160.

Lien, T., Midtbø, R.E., Martinsen, O.J. (2006). Depositional facies and reservoir quality of deep-marine sandstones in the Norwegian Sea. *Norwegian Journal of Geology*, 86, 71–92.

Lowe, D.R. (1982). Sediment gravity flows: II. Depositional models with special reference to the deposits of high-density turbidity currents. *Journal of Sedimentary Petrology* 52, p. 279–297.

Macauley, R. V. and Hubbard, S.M. (2013). Slope channel sedimentary processes and stratigraphic stacking, Cretaceous Tres Pasos Formation slope system, Chilean Patagonia. *Marine And Petroleum Geology* 41: 146-162.

Macdonald, H.A., Peakall, J., Wignall, P.B., Best, J. (2011). Sedimentation in deep-sea lobe elements: implications for the origin of thickening-upward sequences. *Journal of the Geological Society of London* 168, 319–331.

Maino, M., Dallagiovanna, G., Dobson, K., Gaggero, L., Persano, C. Seno, S., Stuart, F.M. (2012). Testing models of orogen exhumation using zircon (U–Th)/He thermochronology: insight from the Ligurian Alps, Northern Italy. *Tectonophysics*, 560–561, 84–93.

Maino, M., Casini, L., Ceriani, A., Decarlis, A., Di Giulio, A., Seno, S., Setti, M., Stuart, F. (2015). Dating shallow thrusts with zircon (U–Th)/He thermochronometry —The shear heating connection, *Geology*, 43, 495-498.

Maino, M. & Seno, S. (2016). The thrust zone of the Ligurian Penninic basal contact (Monte Frontè, Ligurian Alps, Italy). *Journal of Maps*, 12, p. 341-351.

Malgesini, G., Talling, P. J., Hogg, A. J., Armitage, D., Goater, A., Felletti, F. (2015). Quantitative analysis of submarine-flow deposit shape in the Marnoso-Arenacea Formation: what is the signature of hindered settling from dense near-bed layers? *Journal of Sedimentary Research*, 85 (2), 170-191.

Marchand, A.M.E., Apps, G., Li, W., Rotzien, J. R. (2015). Depositional processes and impact on reservoir quality in deepwater Paleogene reservoirs, US Gulf of Mexico: *AAPG Bulletin* 99 (9), 1635–1648.

Marini, M., Milli, S., Ravnås, R. (2015). A comparative study of confined vs. semi-confined turbidite lobes from the Lower Messinian Laga Basin (Central Apennines, Italy): Implications for assessment of reservoir architecture. *Marine And Petroleum Geology*, 62, 142-165.

Marsset, T., Droz, L., Dennielou, B., Pichon, E. (2009). Cycles in the architecture of the quaternary Zaire turbidite system: a possible link with climate. *In: Kneller B., Martinsen O.J., McCaffrey W.D.: External Controls on Deep-Water Depositional Systems*, SEPM Special Publication, 92, pp. 89-106.

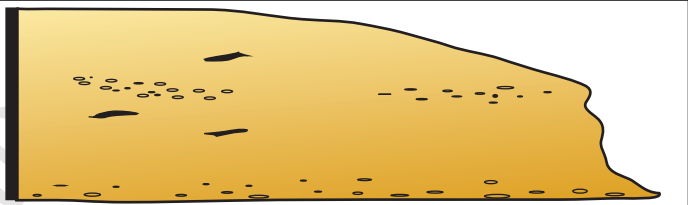
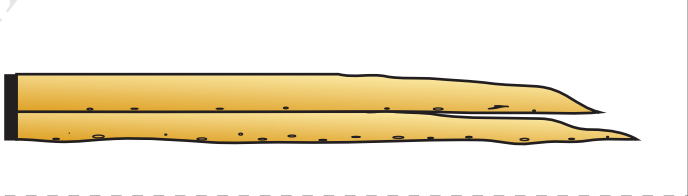
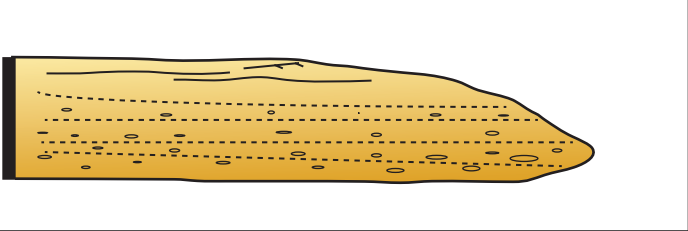
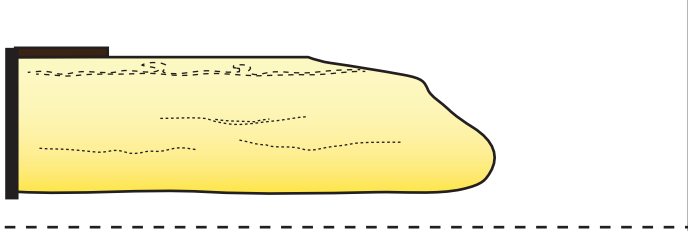
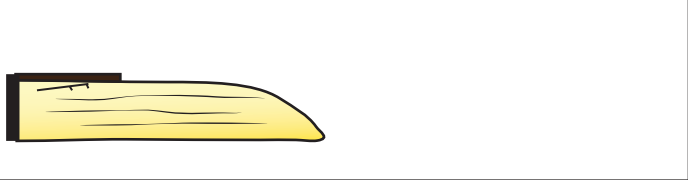
Mattern, F. (2002). Amalgamation surfaces, bed thicknesses, and dish structures in sand-rich submarine fans: numeric differences in channelized and unchannelized deposits and their diagnostic value. *Sedimentary Geology*, 150, 203–228.

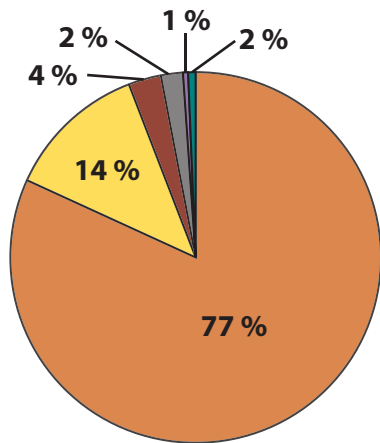
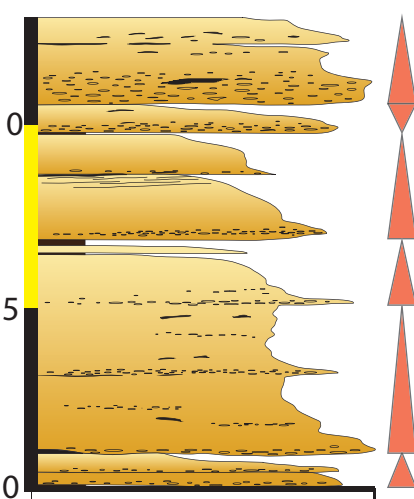
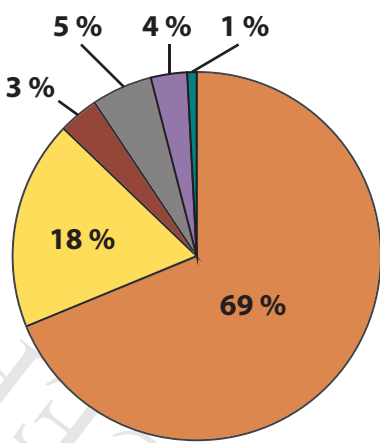
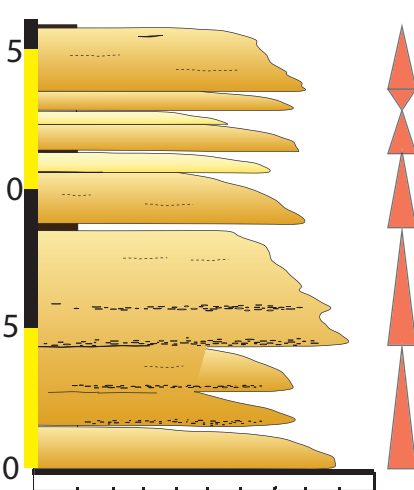
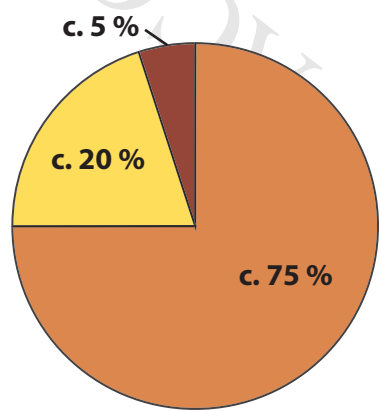
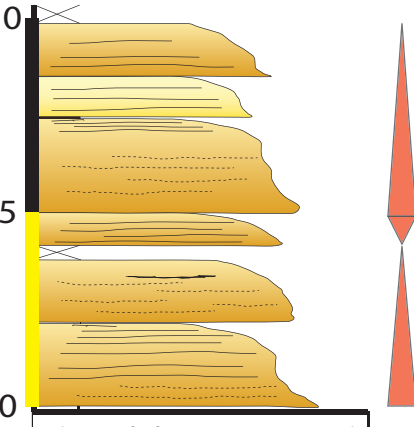
- Mattern, F. (2005). Ancient sand-rich submarine fans: depositional systems, models, identification, and analysis. *Earth-Science Reviews*, 70 (3-4), 167-202.
- McHargue, T., Pyrcz, M.J., Sullivan, M.D., Clark, J., Fildani, A., Romans, B.R., Covault, J.A., Levy, M., Posamentier, H., Drinkwater, N. (2011). Architecture of turbidite channel systems on the continental slope: patterns and predictions. *Marine and Petroleum Geology* 28, 728-743.
- Milli, M. Moscatelli, M., Stanzione, O., Falcini, F. (2007). Sedimentology and physical stratigraphy of the Messinian turbidite deposits of the Laga basin (central Apennines, Italy). *Boll. Soc. Geol. Ital.*, 126, 255–281.
- Morris, E.A., Hodgson, D.M., Flint, S.S., Brunt, R.L., Butterworth, P.L., Verhaeghe, J. (2014). Sedimentology, Stratigraphic Architecture and Depositional Context of Submarine Frontal Lobe Complexes, *Journal of Sedimentary Research* 84, 763-780.
- Mulder, T. & Alexander, J. (2001). The physical character of subaqueous sedimentary density flows and their deposits. *Sedimentology*, 48 (2), 269-299.
- Mulder, T. & Etienne, S. (2010). Lobes in deep-sea turbidite systems, state of the art. *Sedimentary Geology*, 229 (3), 75–80.
- Mulder, T., Callec, Y., Parize, O., Joseph, P., Schneider, J.-L., Robin, C., Dujoncquoy, E., Salles, T., Allard, J., Ducassou, E., Ferger, B., Gaudin, M., Linares, F., Marchés, E., Zaragosi, S. (2010). High-resolution analysis of submarine lobe deposits: seismic-scale outcrops of the Lauzanier area (SE Alps, France). *Sedimentary Geology*, 229, 160–191.
- Mutti, E. & Sonnino, M. (1981). Compensation cycles: a diagnostic feature of turbidite sandstone lobes. In: Valloni, R., Colella, A., Sonnino, M., Mutti, E., Ori, G.G. (Eds.), *Abstr. Int. Assoc. Sediment., 2nd Eur. Reg. Meet., Bologna, Italy*, 120–123.
- Mutti, E. & Normark, W.R. (1987). Comparing examples of modern and ancient turbidite systems: problems and concepts. In: Leggett, J.K., Zuffa, G.G. (Eds.), *Marine Clastic Sedimentology: Concepts and Case Studies*. Graham & Trotman, Oxford, pp. 1–38.
- Mutti, E. & Normark, W.R. (1991). An integrated approach to the study of turbidite systems. In: Weimer, P., Link, M.H. (Eds.), *Seismic Facies and Sedimentary Processes of Submarine Fans and Turbidite Systems*. Springer, New York, pp. 75–106.
- Mutti, E., Tinterri, R., Remacha, E., Mavilla, N., Angella, S., Fava, L. (1999). An introduction to the analysis of ancient turbidite basins from an outcrop perspective. *AAPG Course Notes* 39, 93 pp.
- Muzzi Magalhaes, P. and Tinterri, R. (2010). Stratigraphy and depositional setting of slurry and contained (reflected) beds in the Marnoso-arenacea Formation (Langhian-Serravallian) Northern Apennines, Italy. *Sedimentology* 57(7): 1685-1720.
- Patacci, M. (2016). A high-precision Jacob's staff with improved spatial accuracy and laser sighting capability. *Sedimentary Geology*, 335, 66-69.
- Patacci, M., Haughton, P.D.W., McCaffrey, W.D. (2014). Rheological Complexity in Sediment Gravity Flows Forced to Decelerate against a Confining Slope, Braux, SE France. *Journal of Sedimentary Research*, 84, 270-277.

- Pemberton, E. A. L., Hubbard, S. M., Fildani, A., Romans, B., Stright, L. (2016). The stratigraphic expression of decreasing confinement along a deep-water sediment routing system; outcrop example from southern Chile. *Geosphere* 12(1): 114-134.
- Porten, K.W., Kane, I.A., Warchol, M.J., Southern, S.J. (2016). A Sedimentological Process-Based Approach To Depositional Reservoir Quality of Deep-Marine Sandstones: An Example From the Springar Formation, Northwestern Vøring Basin, Norwegian Sea. *Journal of Sedimentary Research*, 86 (11), p. 1269 -1286.
- Posamentier, H.W., Kolla, V. (2003). Seismic geomorphology and stratigraphy of depositional elements in deep-water settings. *Journal of Sedimentary Research*, 73 (3), 367–388.
- Postma, G., Nemec, W., Kleinspehn, K.L. (1988). Large floating clasts in turbidites: a mechanism for their emplacement. *Sedimentary Geology*, 58, 47–61.
- Postma, G., Cartigny, M., Kleverlaan, K. (2009). Structureless, coarse-tail graded Bouma Ta formed by internal hydraulic jump of the turbidity current? *Sedimentary Geology*, 219 (1), 1–6.
- Postma, G., Kleverlaan, K., Cartigny, M. (2014). Recognition of cyclic steps in sandy and gravelly turbidite sequences and consequences for the Bouma facies model. *Sedimentology*, 61 (7), 2268-2290.
- Powichrowski, L.K. (1989). Trace fossils from the Helminthoid Flysch (Upper Cretaceous-Paleocene) of the Ligurian Alps (Italy): development of deep marine ichnoassociations in fan and basin plain environments. *Eclogae Geologicae Helvetiae* 82, 385-411.
- Prélat, A., Hodgson, D.M., and Flint, S.S. (2009). Evolution, architecture and hierarchy of distributary deep-water deposits: A high-resolution outcrop investigation of submarine lobe deposits from the Permian Karoo Basin, South Africa, *Sedimentology*, 56, 2132–2154.
- Prélat A. & Hodgson D.M. (2013). The full range of turbidite bed thickness patterns in submarine lobes: Controls and implications, *Journal of the Geological Society*, 170, pp.209-214.
- Prélat, A., Covault, J.A., Hodgson, D.M., Fildani, A., Flint, S.S. (2010). Intrinsic controls on the range of volumes, morphologies, and dimensions of submarine lobes: *Sedimentary Geology*, 232, 66–76.
- Pringle, J.K., Brunt, R.L., Hodgson, D.M., Flint, S.S. (2010). Capturing stratigraphic and sedimentological complexity from submarine channel complex outcrops to digital 3D models, Karoo Basin, South Africa. *Petroleum Geoscience*, 16, 307-330.
- Romans, B.W., Hubbard, S.M., Graham, S.A. (2009). Stratigraphic evolution of an outcropping continental slope system, Tres Pasos Formation at Cerro Divisadero, Chile. *Sedimentology* 56, 737-764.
- Rotzien, J.R., Lowe, D.R., Schwalbach, J.R. (2014). Processes of Sedimentation and Stratigraphic Architecture of Deep-Water Braided Lobe Complexes: The Pliocene Repetto and Pico Formations, Ventura Basin, U.S.A. *Journal of Sedimentary Research*, 84 (19), 910-934.
- Russell, H.A.J., Arnott, R.W.C. (2003). Hydraulic-jump and hyperconcentrated-flow deposits of a glacial subaqueous fan: oak ridges moraine, southern Ontario, Canada. *Journal of Sedimentary Research* 73 (6), 887–905.

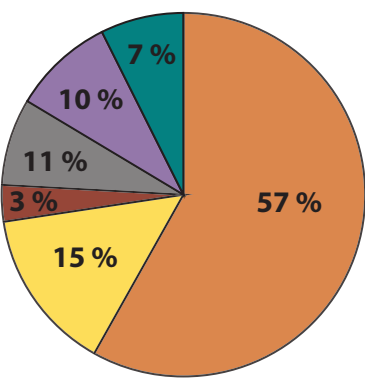
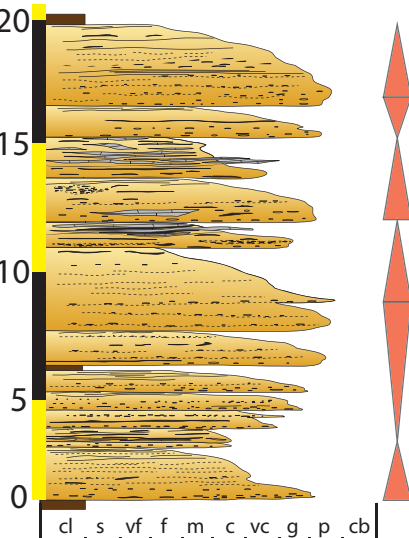
- Sagri, M. (1980). Le Arenarie di Bordighera: una conoide sottomarina nel bacino di sedimentazione dei Flysch ad Elmintoidi di San Remo (Cretaceo Superiore, Liguria Occidentale). *Bollettino della Società Geologica Italiana* 98-99, 205-226.
- Saller, A.H., Werner, K., Sugiawan, F., Cebastian, A., May, R., D. Glenn, D., Barker, C. (2008). Characteristics of Pleistocene deep-water fan lobes and their application to an Upper Miocene reservoir model, offshore East Kalimantan, Indonesia. *AAPG Bulletin*, 92, 919-949.
- Satur, N., Kelling, G., Cronin, B. T., Hurst, A. and Gurbuz, K. (2005). Sedimentary architecture of a canyon-style fairway feeding a deep-water clastic system, the Miocene Cingoz Formation, southern Turkey: significance for reservoir characterisation and modelling. *Sedimentary Geology* 173 (1-4): 91-119.
- Slaczka, A. & Thompson, S. III (1981). A revision of the fluxoturbidite concept based on type examples in the Polish Carpathian flysch. *Ann. Soc. Geol. Pologne* 51, 3-44.
- So, Y.S., Rhee, C.W., Choi, P.-Y., Kee, W.-S., Seo, J.Y., Lee, E.-J. (2013). Distal turbidite fan/lobe succession of the Late Paleozoic Taean formation, western Korea. *Geoscience Journal*, 17, 9–25.
- Sohn, Y.K. (1997). On traction-carpet sedimentation. *Journal of Sedimentary Research*, 67, 502–509.
- Sohn, Y.K., Choe, M.Y., Jo, H.R. (2002). Transition from debris flow to hyperconcentrated flow in a submarine channel (the Cretaceous Cerro Toro Formation, southern Chile). *Terra Nova*, 14, 405-415.
- Southard, J.B. & Bogouchal, L.A. (1990). Bed configurations in steady unidirectional water flows. Part 2. Synthesis of flume data. *Journal of Sedimentary Petrology*, 60, 658–679.
- Spychala, Y.T., Hodgson, D.M., Prélat, A., Kane, I.A., Flint, S.S., Mountney, N. (2017). Frontal and lateral submarine lobe fringes: comparing sedimentary facies, architecture and flow processes. *Journal of Sedimentary Research*, 87, 1–21.
- Southern, S. J., Patacci, M., Felletti, F., McCaffrey, W. D. (2015). Influence of flow containment and substrate entrainment upon sandy hybrid event beds containing a co-genetic mud-clast-rich division. *Sedimentary Geology* 321, 105-122.
- Southern, S.J., Kane, I.A., Warchoń, M.J., Porten, K.W., McCaffrey, W.D. (2016). Hybrid event beds dominated by transitional-flow facies: Character, distribution and significance in the Maastrichtian Springar Formation, north-west Vøring Basin, Norwegian Sea. *Sedimentology*: DOI: 10.1111/sed.12323
- Stanbrook, D., Bentley, M., Stephens, E. (2015). Controls on Architectural Styles in Turbidite Systems: The Role of Relative Confinement. *Asia Petroleum Geoscience Conference & Exhibition (APGCE) conference extended abstracts*.
- Stevenson, C.J., Jackson, C. A.-L., Hodgson, D.M., Hubbard, S.M., Eggenhuisen, J.T. (2015). Deep-Water Sediment Bypass. *Journal of Sedimentary Research*, 85 (9), 1058-1081.
- Stow, D.A.V. & Johansson, M. (2000). Deep-water massive sands: nature, origin and hydrocarbon implications. *Marine and Petroleum Geology*, 17, 145-174.
- Sumner, E.J., Talling, P.J., Amy, L.A. (2009). Deposits of flows transitional between turbidity current and debris flow. *Geology*, 37, 991-994.
- Sylvester, Z. & Lowe, D.R. (2004). Textural trends in turbidites and slurry beds from the Oligocene flysch of the East Carpathians, Romania. *Sedimentology*, 51 (5), 945-972.

- Talling, P.J., Masson, D.G., Sumner, F.J., Malgesini G. (2012). Subaqueous sediment density flows: Depositional processes and deposit types. *Sedimentology*, 59, 1937–2003
- Terlaky, V. & Arnott, R.W.C. (2014). Matrix-rich and associated matrix-poor sandstones: avulsion splays in slope and basin-floor strata. *Sedimentology*, 61 (5), 1175-1197.
- Terlaky, V., Rochelau, J., Arnott, R.W.C. (2015). Stratal composition and stratigraphic organization of stratal elements in an ancient deep-marine basin-floor succession, Neoproterozoic Windermere Supergroup, British Columbia, Canada. *Sedimentology* 63, 136-175.
- Terlaky, V. & Arnott, R.W.C. (2016). The Control Of Terminal-Splay Sedimentation On Depositional Patterns and Stratigraphic Evolution In Avulsion-Dominated, Unconfined, Deep-Marine Basin-Floor Systems. *Journal of Sedimentary Research* 86 (7): 786-799.
- Uchman, A. (2007). Deep-sea trace fossils from the mixed carbonate-siliciclastic flysch of the Monte Antola Formation (Late Campanian-Maastrichtian), North Apennines, Italy. *Cretaceous Research*, 28, 980-1004.
- Underwood, M.B., Orr, R., Pickering, K., Taira, A. (1993). Provenance and dispersal patterns of sediments in the turbidite wedge of Nankai Trough. In: Hill, I.A., Proceedings of the Ocean Drilling Program, Scientific results, 131, College Station, Texas, Ocean Drilling Program, 15–34.
- Vanossi M., Cortesogno L., Galbiati B., Messiga B., Piccardo G., Vannucci R. (1986). Geologia delle Alpi liguri: dati, problemi, ipotesi. *Memorie della Società Geologica Italiana* 28, 5–75.
- Weimer, P., Slatt, R.M., Pettingill, H.S. (2007). Global Overview of Deepwater Exploration and Production. In: Weimer, P. and Slatt, R. M. (Eds). Introduction to the Petroleum Geology of Deepwater Settings. *AAPG Studies in Geology* 57: 19-56.
- Wynn, R.B., Kenyon, N.H., Masson, D.G., Stow, D.A.V., Weaver, P.P.E. (2002). Characterization and recognition of deep-water channel-lobe transition zones. *AAPG Bulletin* 86, 1441-1462.

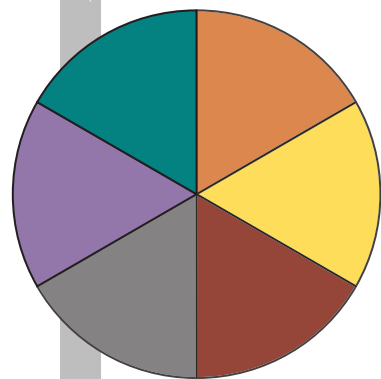
BT	Description and interpretation	Geometry (10s of m)	c l a s t i c s i l t s t o n e s v f s s t f s s t m i c r i t e s c a l c a r e o u s s a n d s t o n e s g r a n u l a r c o n g l o m e r a t e s p e b b l e s
1.1	<p>Medium- to very thick-bedded, coarse-tail graded microconglomerates. Absence of stratifications. Common dewatering dishes and sheets. Sporadic loading structures. Frequent amalgamations. Maximum basal grain size: angular pebbles. Minor portions of mud-clasts. Thickness: 0.45-5.87 m; mean: 1.35 m.</p> <p>Interpretation: Hyperconcentrated density flows (Mulder & Alexander, 2001)</p>	lenticular / tabular	
1.2	<p>Thin-bedded structureless clast-supported microconglomerates. Granule- to small pebbles in coarse to very coarse sandy matrix. Matrix typified by general absence of clay. Abrupt normal grading towards tops of beds. Very rare basal inverse grading. Thickness: 0.12-0.45 m; mean: 0.30 m.</p> <p>Interpretation: Non-cohesive debris flows (Mulder & Alexander, 2001)</p>	tabular	
1.3	<p>Medium- to thick-bedded inversely graded microconglomerates. Inverse basal grading followed by well-developed, continuous normal grading. Beds are structureless or show a range of primary physical structures (clast imbrications, cross-stratifications, planar-parallel, wavy and current-ripple laminations). Rapid grain size jumps. Thickness: 0.35-2.45 m; mean: 0.85 m.</p> <p>Interpretation: High density turbidity currents (S1 & S3 of Lowe, 1982)</p>	lenticular / tabular	
2.1	<p>Thin- to thick-bedded, graded structureless sandstones. Common fluid escape structures (dewatering dishes and deformed dewatering sheets). Absence of sedimentary structures resulting from traction processes. Minor proportions of intraformational siliciclastic and calcareous rip-up clasts. Thickness: 0.07-2.20 m; mean: 0.50 m.</p> <p>Interpretation: High- to low-density turbidity currents (S3 of Lowe, 1982)</p>	lenticular / tabular	
2.2	<p>Thin- to thick-bedded, graded structured sandstones. Sedimentary structures (planar-parallel and cross laminations; climbing ripples) restricted to medial and upper parts of beds. Intense convolute laminations. Very rare rip-up clasts. Thickness: 0.10-1.55 m; mean: 0.50 m.</p> <p>Interpretation: Low density turbidity currents (Mulder & Alexander, 2001)</p>	lenticular / tabular	
3	<p>Heterolithic intervals (clastic & calcareous fine beds): mudstones, calcareous micrites, siltstones, vfsst to fsst & micrites. Wavy- to ripple laminations, rare planar laminations. Abundant trace fossils. Sst soles: <i>Gordia</i>, <i>Ophiomorpha</i>, <i>Planolites</i>. Calcareous beds: <i>Nereites</i>, <i>Chondrites</i>, <i>Thalassinoides</i>, <i>Urohelminthoides</i>. Thickness 0.12-3.10 m; mean: 0.40 m.</p> <p>Interpretation: Low density turbidity currents (Mulder & Alexander, 2001)</p>	tabular	
4	<p>Medium- to thick-bedded calcilutites & calcarenites. Either ripple-laminated or structure-less appearance. Locally meter-scale injections of coarse sst (max. ca. 35 cm x 6.5 m). Abundant "Helminthoid" traces at soles: <i>Nereites irregularis</i>, <i>Chondrites</i>, <i>Urohelminthoides</i>; <i>Ophiomorpha</i> & <i>Planolites</i>. Thickness 0.03-2.25 m; mean: 0.25 m.</p> <p>Interpretation: Low density turbidity currents (Mulder & Alexander, 2001)</p>	tabular	

BTA	Descriptive characteristics, geometries, thicknesses	AR, Sand-to-mud	BT proportions	Typical Motif
1.1: Channel axis Representative section: Badalucco-Quarry. GPS: 43.886135, 7.846541	<p>Homogeneous sand bodies characterised by mud-poor massive, commonly structureless thick- to very thick-bedded microconglomerates and medium- to very coarse-grained "clean" sandstones. Subordinate presence of clean sandstones with primary sedimentary structures. Scarcity of heterolithic intervals. Very rare calcareous strata and beds enriched in mud-clasts and HEBs. Both tabular and lenticular bedset geometries (outcrop-scale). Lenticular bedsets portray generally low erosional depth (dm-scale; mean ca. 10-15 cm). Bedsets (thickness ca. 5-35 m) commonly organized in fining-up sequences.</p> <p>Amalgamated intervals thicknesses 0.8 m - 14.5 m (average 3.2 m). Paleocurrent data: unidirectional sediment dispersal ($350^\circ \pm 20^\circ$; n=10).</p>	AR: ca. 75 % Sand-to-mud: 11 : 1 		
1.2: channel off-axis Representative section: Monte Bignone. GPS: 43.866230 / 7.748397	<p>Predominance of medium- to thick-bedded, "clean" bed types. Increase in bed types with primary sedimentary structures and decrease in mean max. grain size in comparison to BTA 1.1. Increase in presence of heterolithic intervals.</p> <p>Either lenticular or tabular bed geometries (outcrop-scale). Bedsets internally arranged in fining-upward cycles (thickness 5-25 m), commonly separated by heterolithic drapes.</p> <p>Amalgamated intervals thicknesses 0.7 m - 6.5 m (average 3 m). Comparably unidirectional paleocurrent dispersal ($360^\circ \pm 25^\circ$; n = 14).</p>	AR: ca. 60 % Sand-to-mud: 4 : 1 		
1.3: Distributary channel Representative section: Farenga: GPS 44.082924, 7.734712	<p>Predominance of medium- to thick-bedded "clean" bedsets. Exclusive distribution in the distal domain of the sediment fairway.</p> <p>Slightly lenticular geometries (outcrop-scale), portraying small-scale incisions (< 25 cm) into underlying surfaces. Fining-up and thinning-up bedset patterns.</p> <p>Bed set thickness ca. 2 m - 15 m (average 5 m); Estimated width: ca. 300-400 m. Unidirectional paleocurrent dispersal ($15^\circ \pm 10^\circ$; n = 4).</p>	AR: ca. 85 % Sand-to-mud: 9 : 1 		

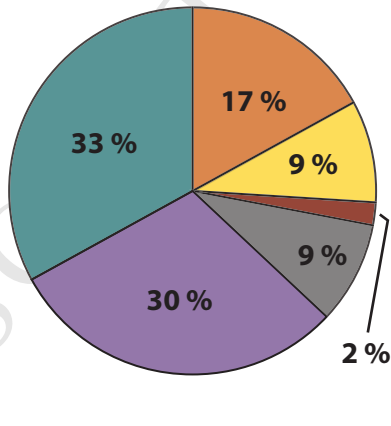
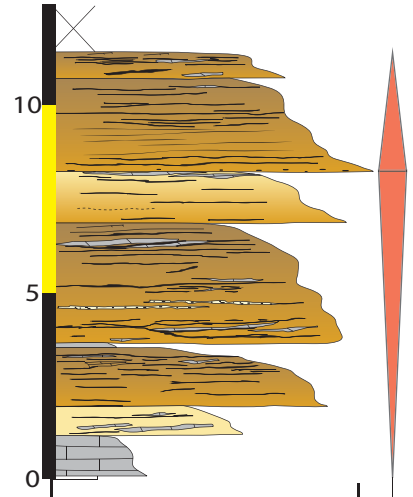
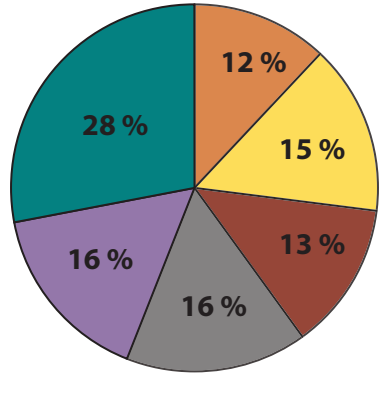
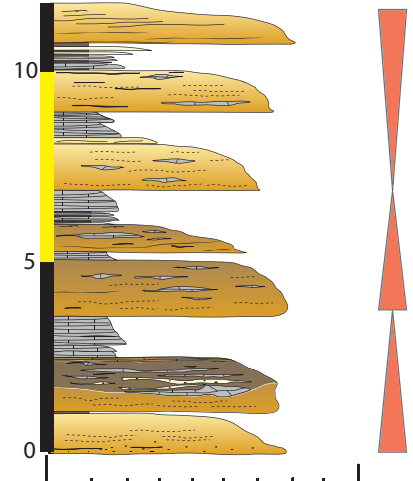
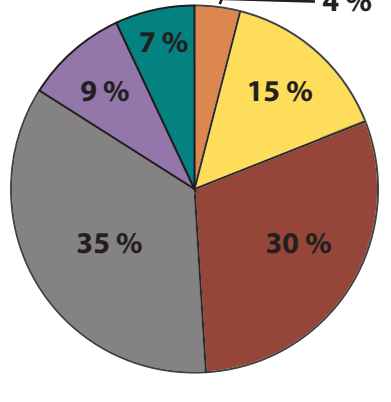
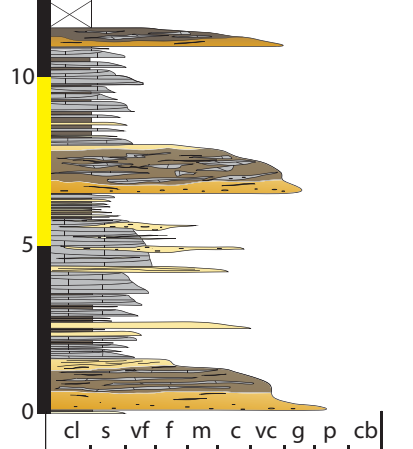
cl s vf f m c vc g p cb

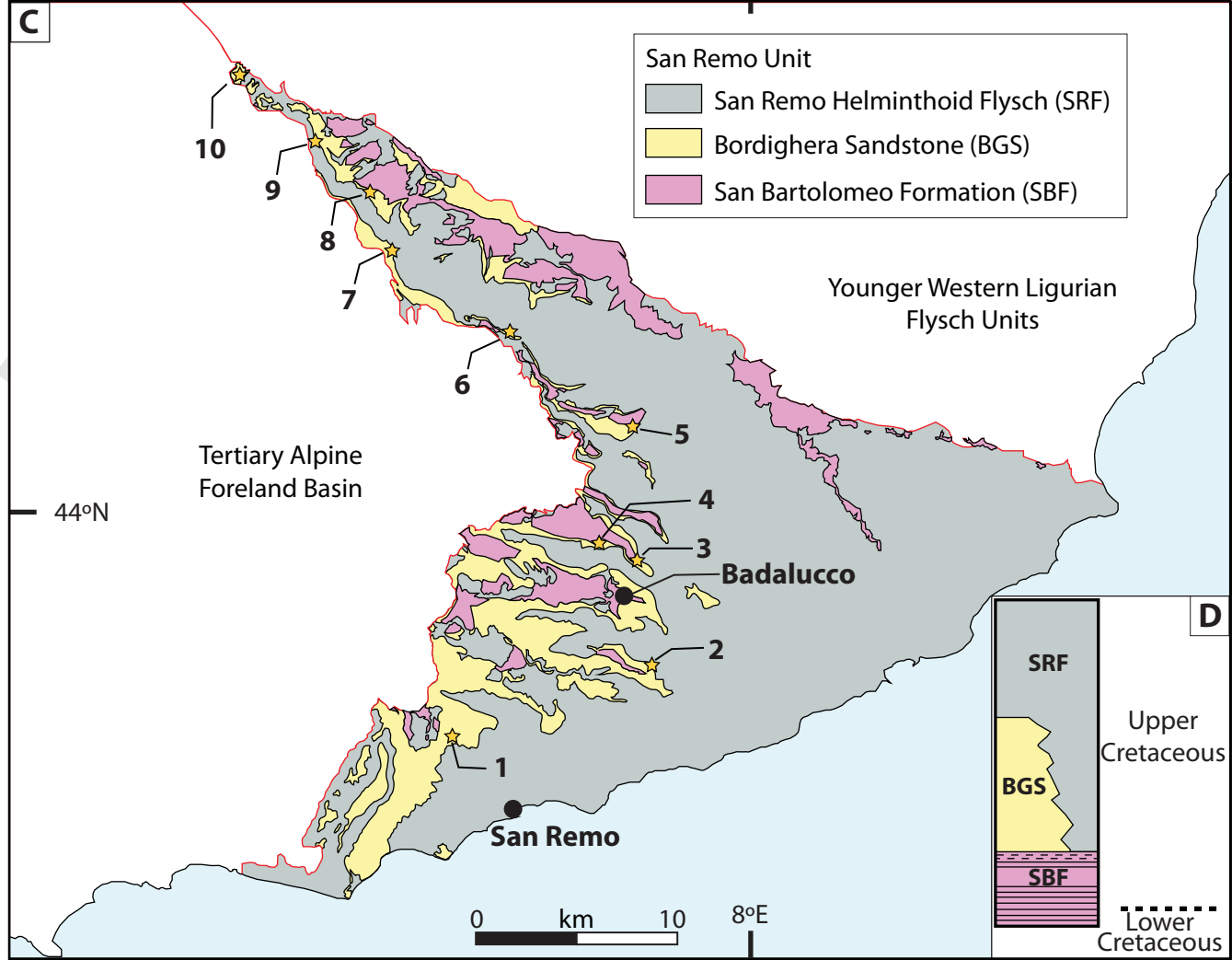
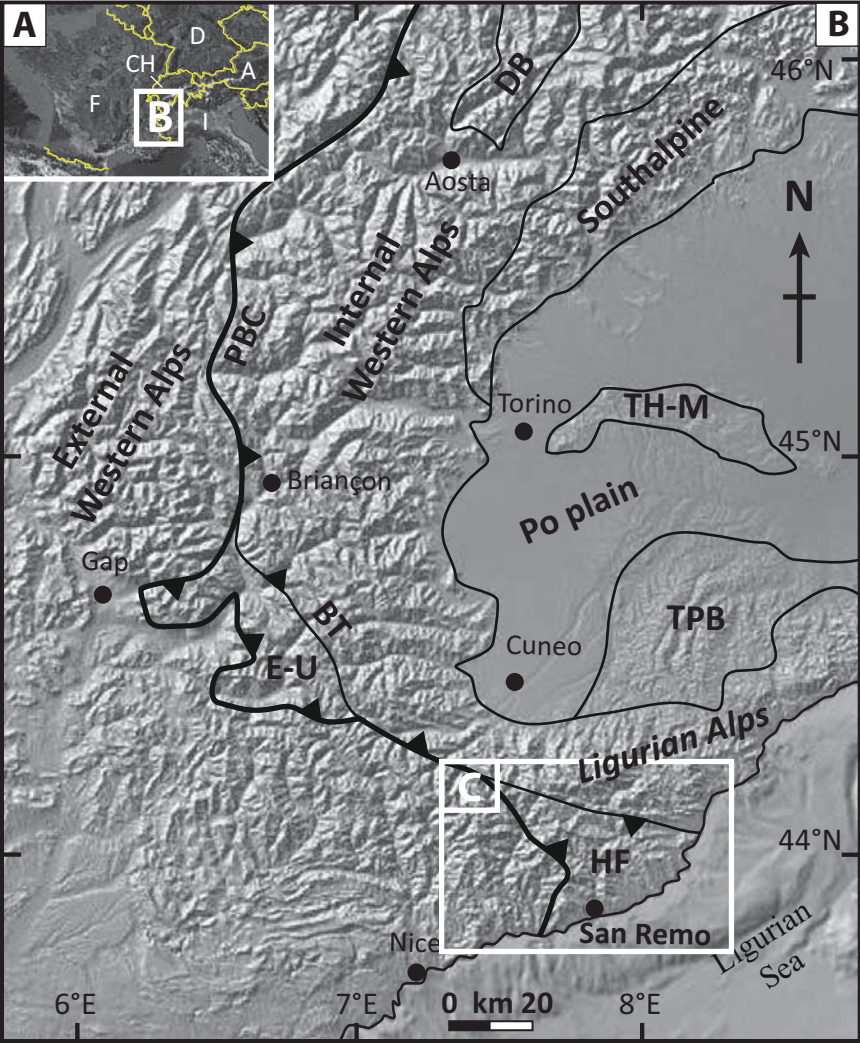
BTA	Description	AR, Sand-to-mud	BT proportions	Typical Motif
2: Composite channelized / tabular association	<p>Predominance of thick-bedded strata of "mixed" bed type proportions, including a variety of "clean" (mud-poor) and "dirty" (mud-rich) bed types. Common tabular scours. Local presence of microconglomeratic lags.</p> <p>Both lenticular and tabular bedset geometries; greater abundance of tabular bedset geometries. Bed sets (thickness 4 m - 25 m) separated by muddy and heterolithic intervals. No clear trends in fining-upward or coarsening-upward patterns.</p> <p>Amalgamated intervals thicknesses: 0.75 m - 23.5 m (average 4 m). Paleocurrent data: comparably high dispersal range (standard deviation of $\pm 76^\circ$). Mean vector of paleocurrent orientation is 308° (n = 36).</p>	<p>AR: 65 - 70 %</p> <p>Sand-to-mud: 6 : 1</p> 		

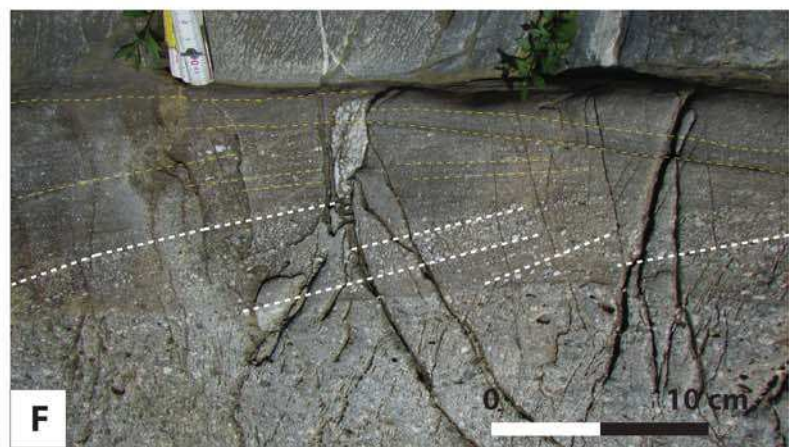
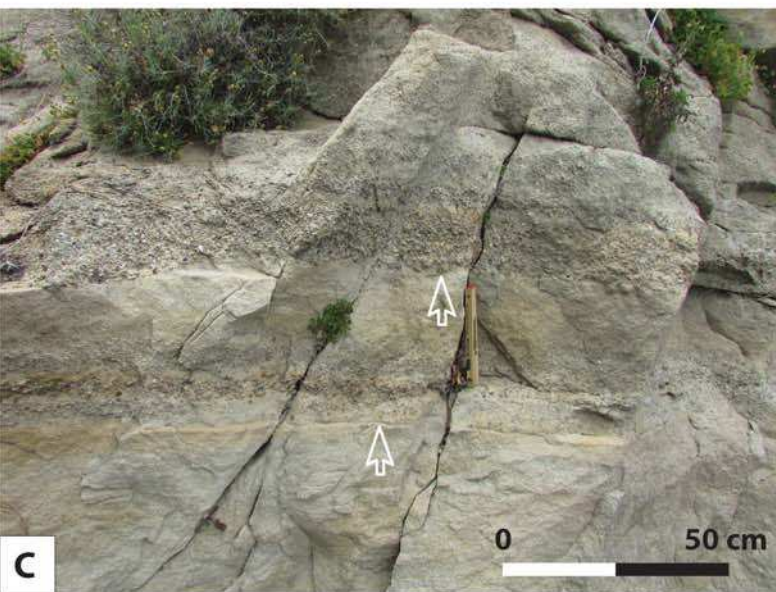
Pie-chart legend

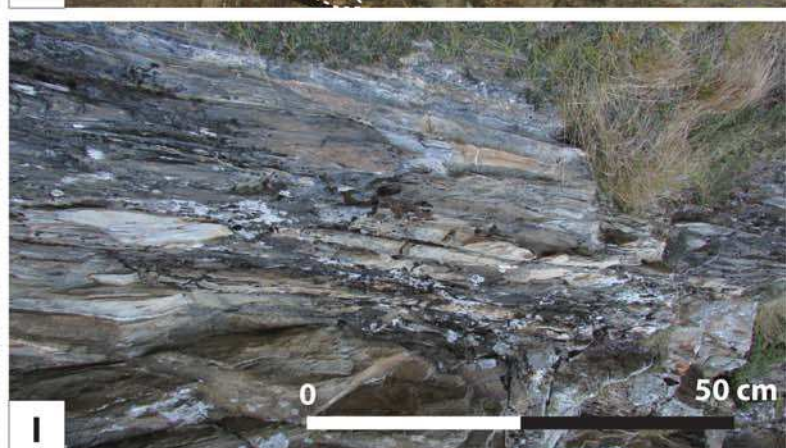
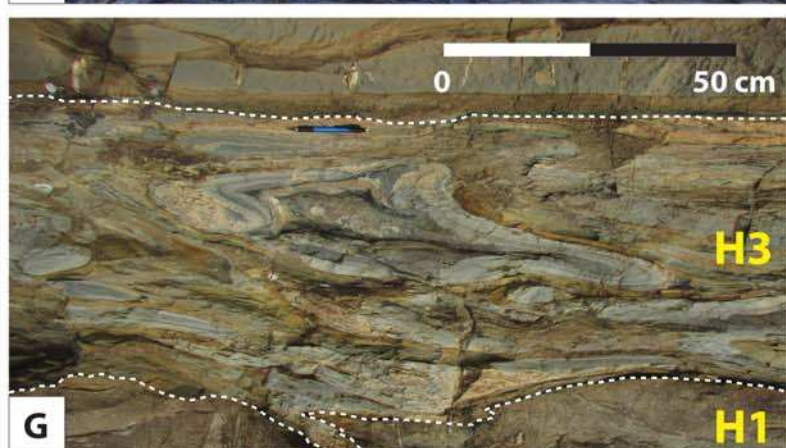
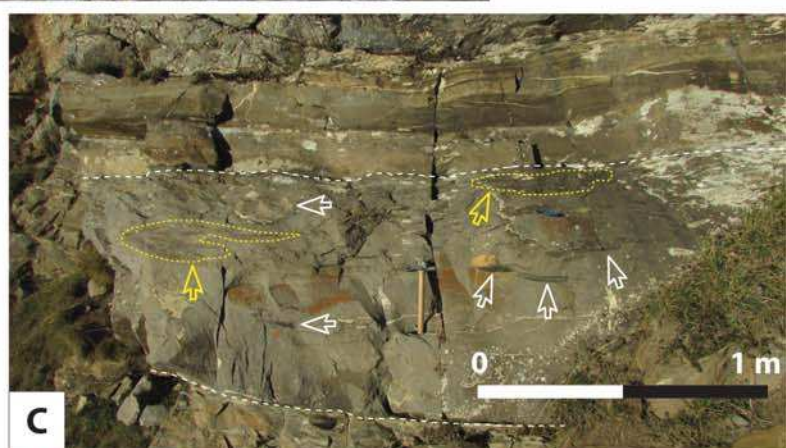
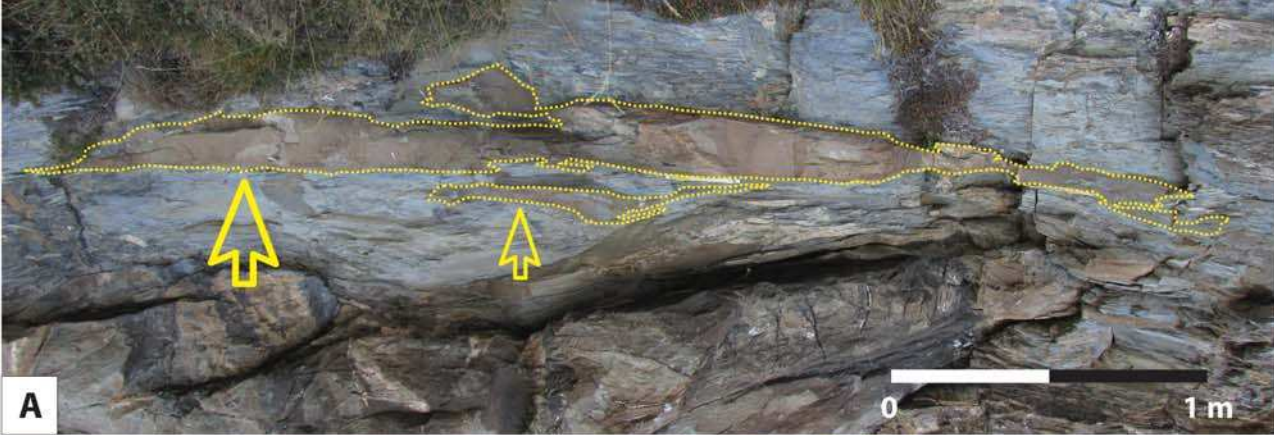


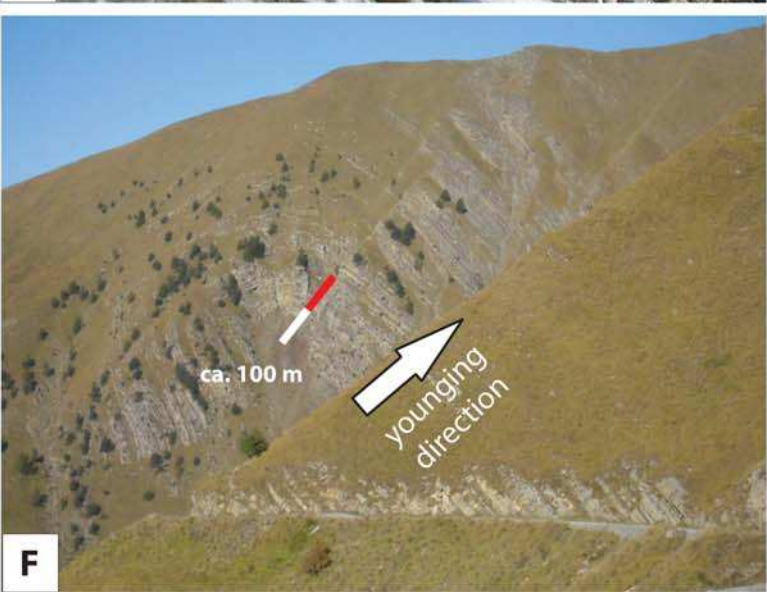
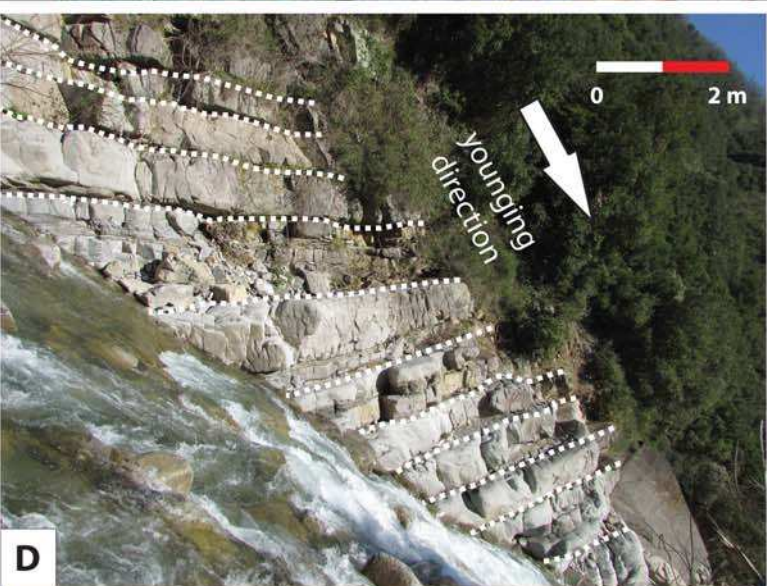
-  Microconglomerates (Bed type 1)
-  Sandstones (Bed type 2)
-  Heterolithic intervals (Bed type 3)
-  Calcareous mudstones (Bed type 4)
-  Mud-clast sandstones (Bed type 5)
-  Hybrid event beds (Bed type 6)

BTA	Description	AR, Sand-to-mud	BT proportions	Typical Motif
3.1: Axial / proximal lobe Representative section: Monte Frontè. GPS: 44.045383, 7.752036	<p>Predominance of medium- to thick-bedded strata enriched in mudclasts and hybrid event beds. Reduced proportions of "clean" bed types. Infrequent intercalations of heterolithic intervals. Increase of proportions of calcareous beds.</p> <p>Prevalent coarse basal grain sizes; max. small to medium-sized pebbles.</p> <p>Good lateral continuity (outcrop-scale). Stratal geometry of beds exclusively tabular. Large-scale coarsening-up trends followed by a large-scale fining-up pattern. Thicknesses of high sand-to-mud bedsets ca. 10 m - 25 m. Bedsets separated by thin calcareous muddy intervals. Amalgamated intervals thicknesses 1.1 m - 8.3 m, average thickness ca. 3.2 m. Paleocurrent data: high dispersal range (mean orientation: 35°; ± 51°).</p>	AR: > 55 % Sand-to-mud: 5.5 : 1		
3.2: Off-axis lobe Representative section: Carmo dei Brocchi. GPS: 44.004020, 7.802283	<p>Balanced ratios of bed types. Marked decrease in individual bed thicknesses in comparison to bed type association 3.1. Reduced proportions of mudclast-rich bed types. Sand-rich intervals separated by heterolithic and calcareous trata. Maximum basal grain size coarse granules.</p> <p>Most beds have a tabular geometry at the outcrop scale (10s m). Sand-rich intervals commonly organized in alternating coarsening-up and fining up cycles. Bed set thicknesses ca. 1 m - 7 m. Reduced amalgamation ratios.</p> <p>Amalgamated intervals thicknesses: 0.2 m - 5.5 m; average thickness ca. 2.5 m. Paleocurrent data: comparably high dispersal range typified by a circular deviation of ±42°. The mean orientation is that of 28° (n = 7).</p>	AR: < 30 % Sand-to-mud: 1.5 : 1		
3.3: Intra-lobe / lobe fringe Representative section: Briga Alta. GPS: 44.085244, 7.755024	<p>Predominant proportions of thin- to medium-bedded heterolithic and calcareous bed types. Within individual heterolithic intervals, fine-grained sandstones and siltstones typically display current-ripple laminations. Local occurrence of medium-bedded hybrid event beds.</p> <p>Increase in calcareous beds proportion. Increasing thickness of calcareous strata and bioturbation with further distance from high sand-to-mud intervals.</p> <p>Stratal geometries are generally tabular, with no evidence of basal erosion. Rare to absent amalgamations.</p>	AR: << 5 % Sand-to-mud: < 0.5 : 1		









A**Bed Amalgamation (BA)****Bed Types Associations (BTA)****Bed Types (BT)**

5.1

Mudclast-rich bed (<10% mudclasts)

5.2

Mudclast-rich bed (>10% mudclasts)

6.2

HEB (bipartite, sharp)

6.1

HEB (tripartite, sharp)

6.3

HEB (bipartite, gradational)

Silt and mud (calcareous)

Silt and mud (siliciclastic)

Covered interval

amalgamated

not amalgamated

- 1.1 Axial channel
- 1.2 Channel off-axis
- 1.3 Distributary channel
- 2 Composite association
- 3.1 Axial/proximal lobe
- 3.2 Lobe off-axis
- 3.3 Inter-lobe

- 1.1 Coarse-tail graded microconglomerate
- 1.2 Microconglomeratic lag
- 1.3 Inversely graded microconglomerate
- 2.1 Structureless "clean" sandstone
- 2.2 Structured "clean" sandstone

★ Log 1

★ Log 4

★ Log 6

★ Log 3

★ Log 5

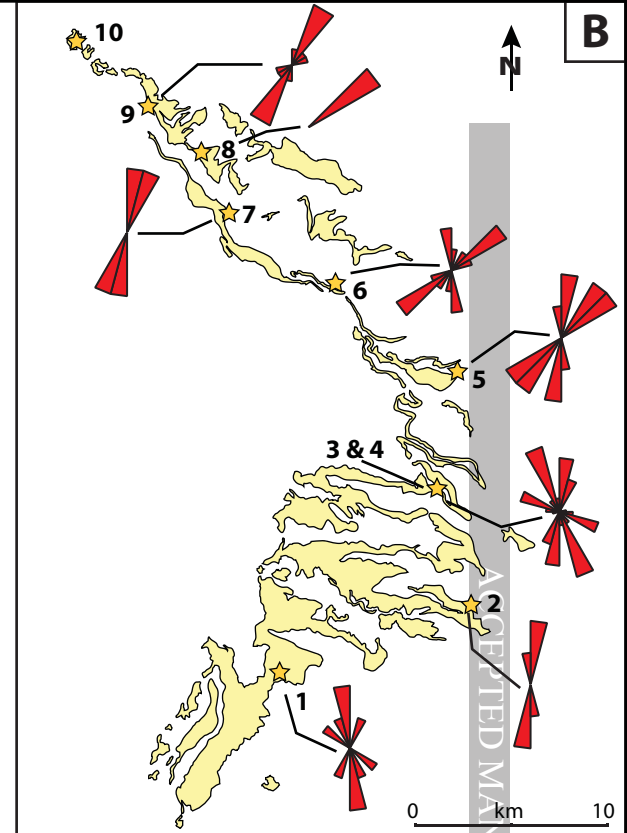
★ Log 9

★ Log 8

★ Log 7

★ Log 10

Datum (limit Bordighera Sandstones/San Bartolomeo Formation)

B

ACCEPTED MANUSCRIPT

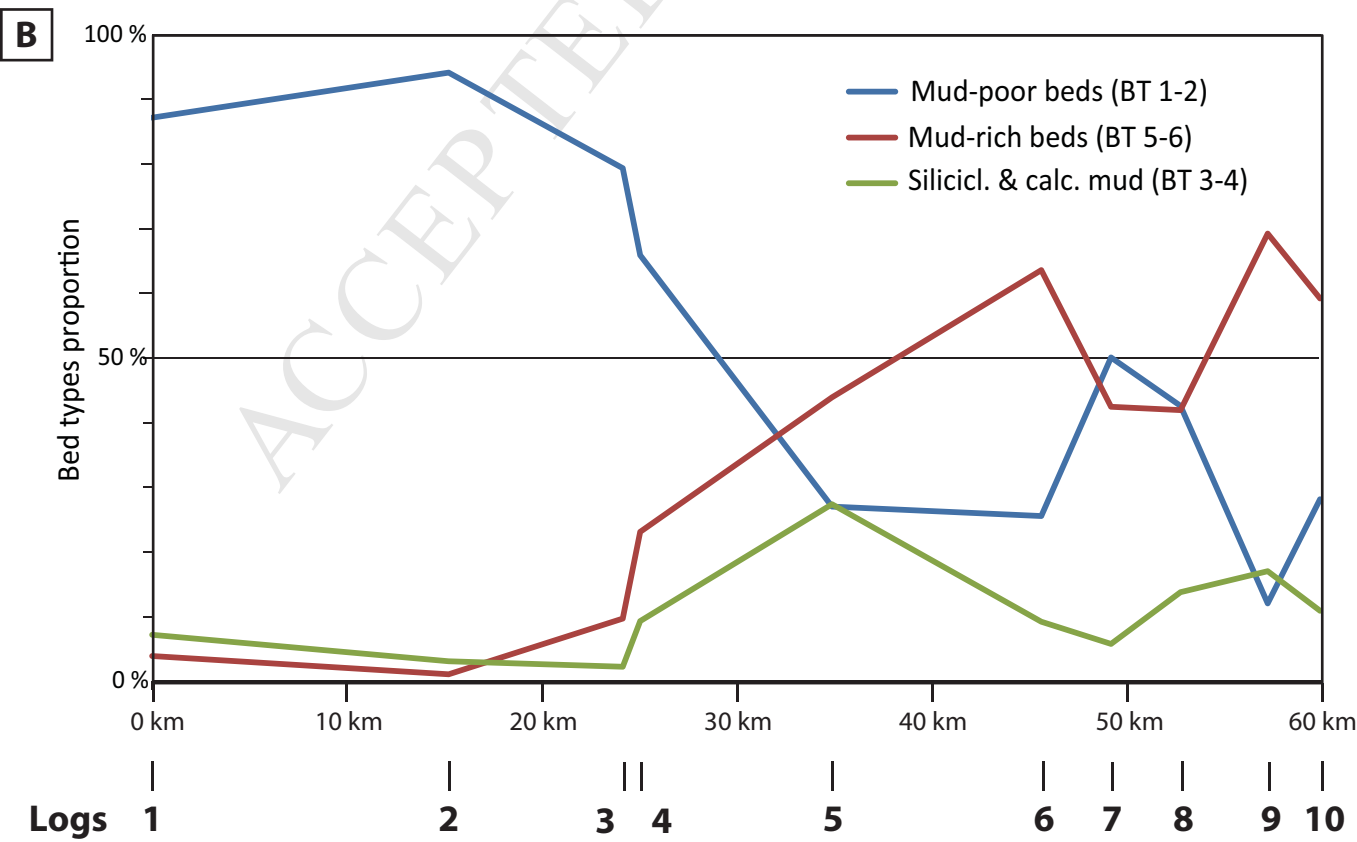
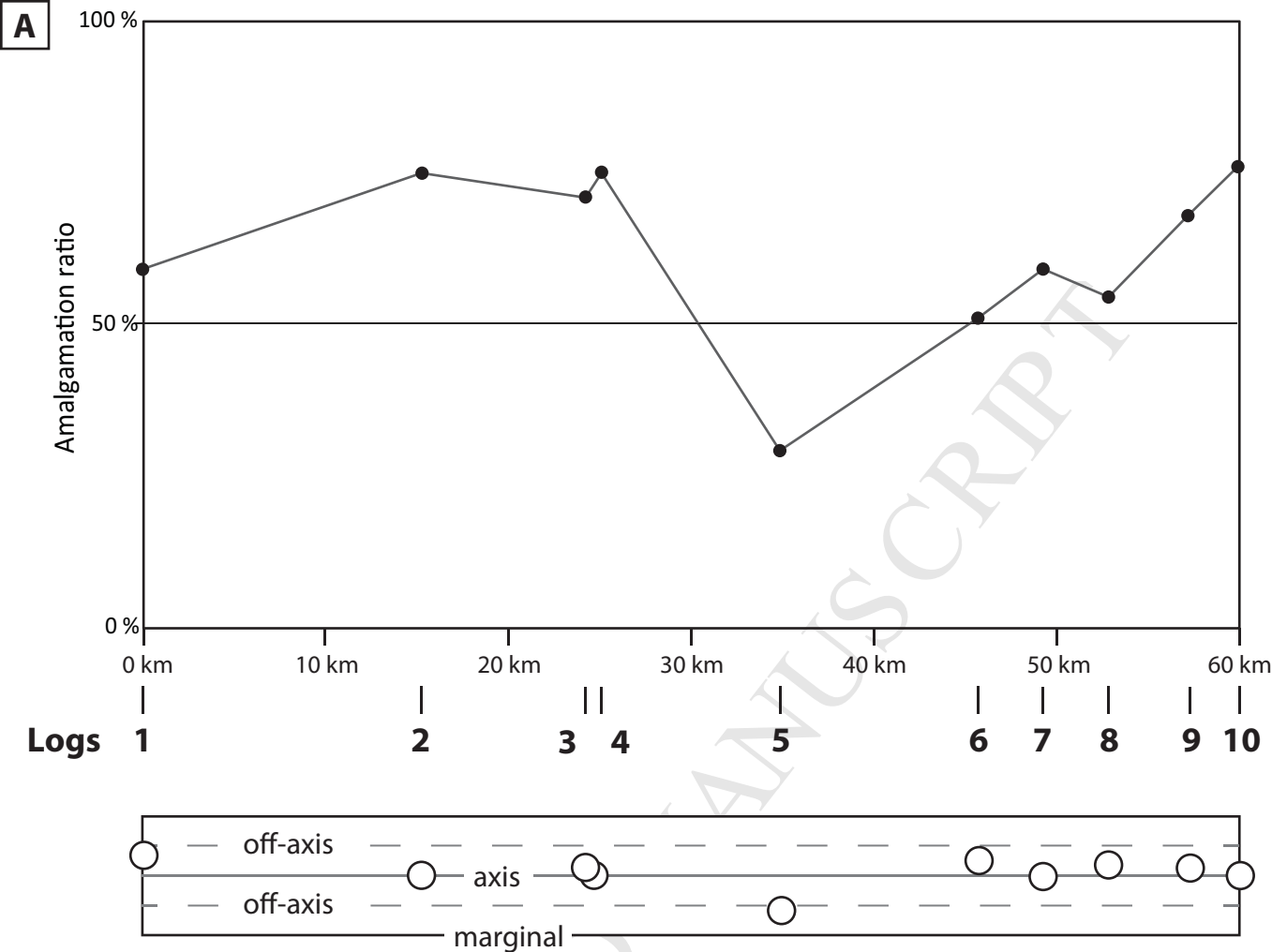
clay

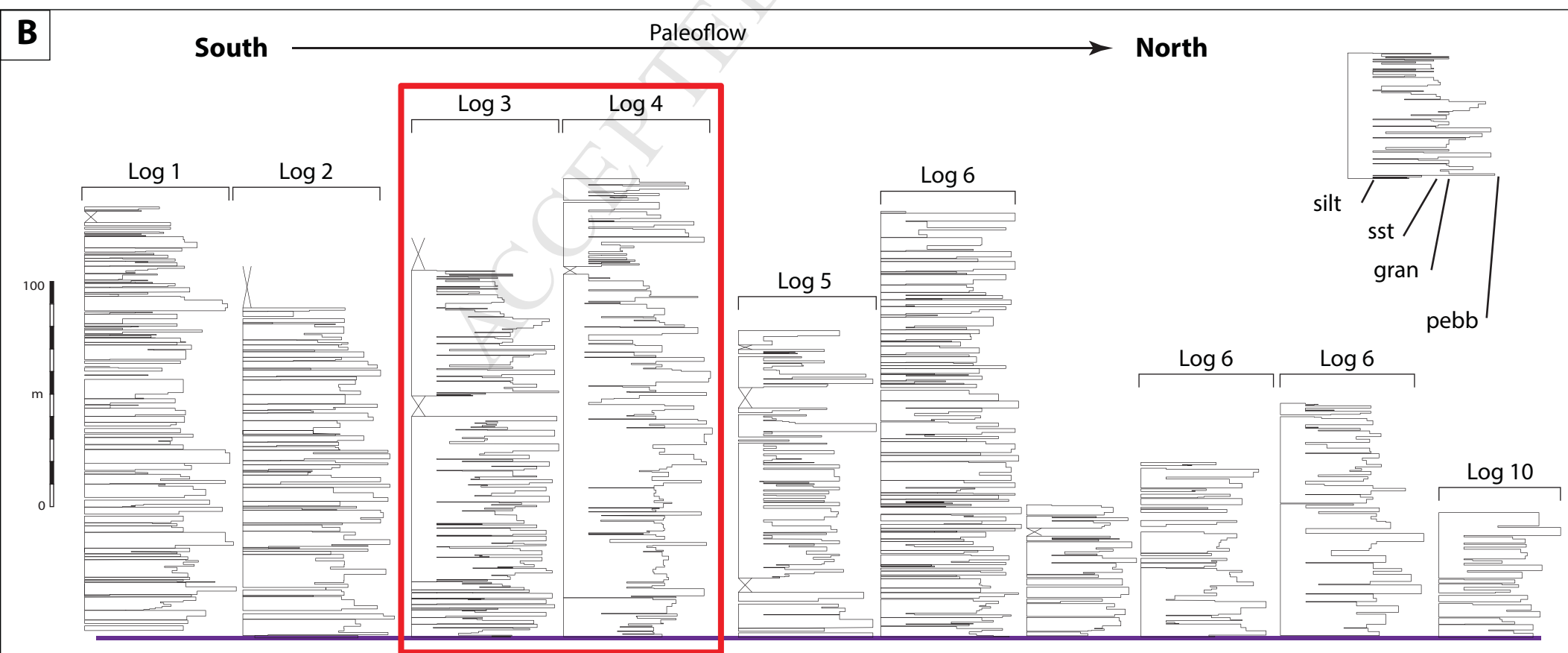
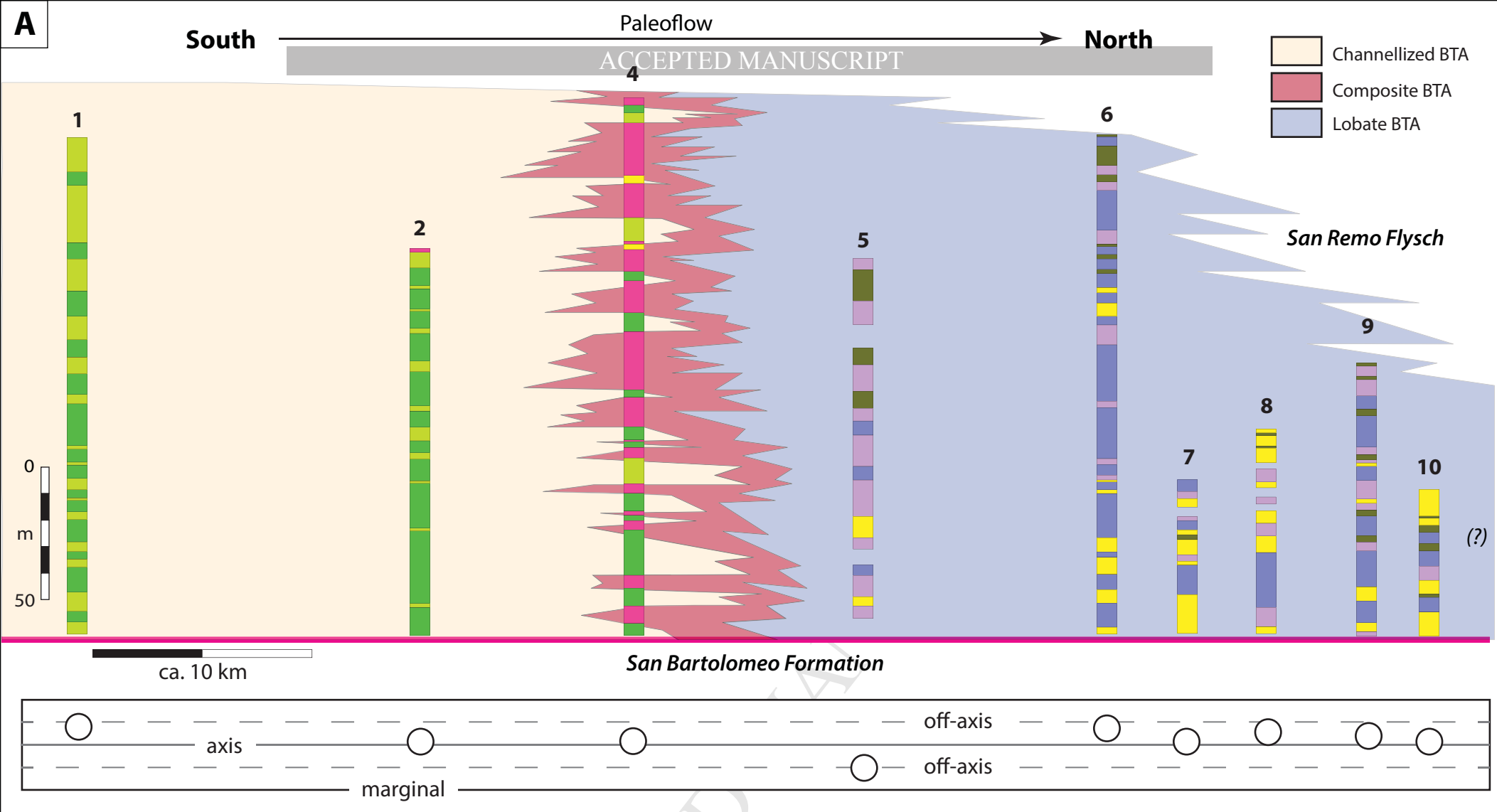
silt

ms

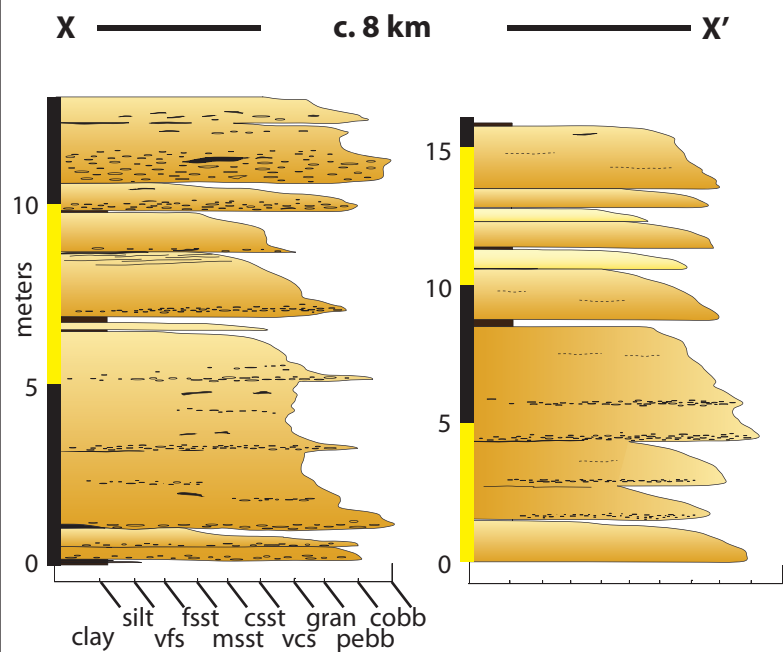
vcs

pebb

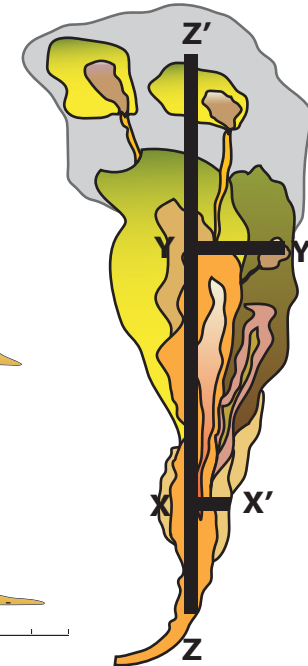
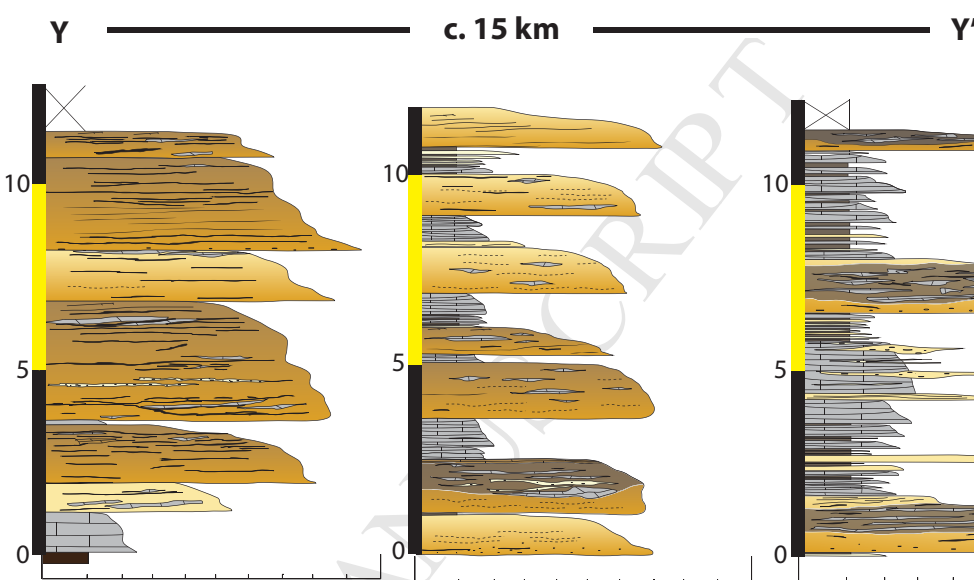




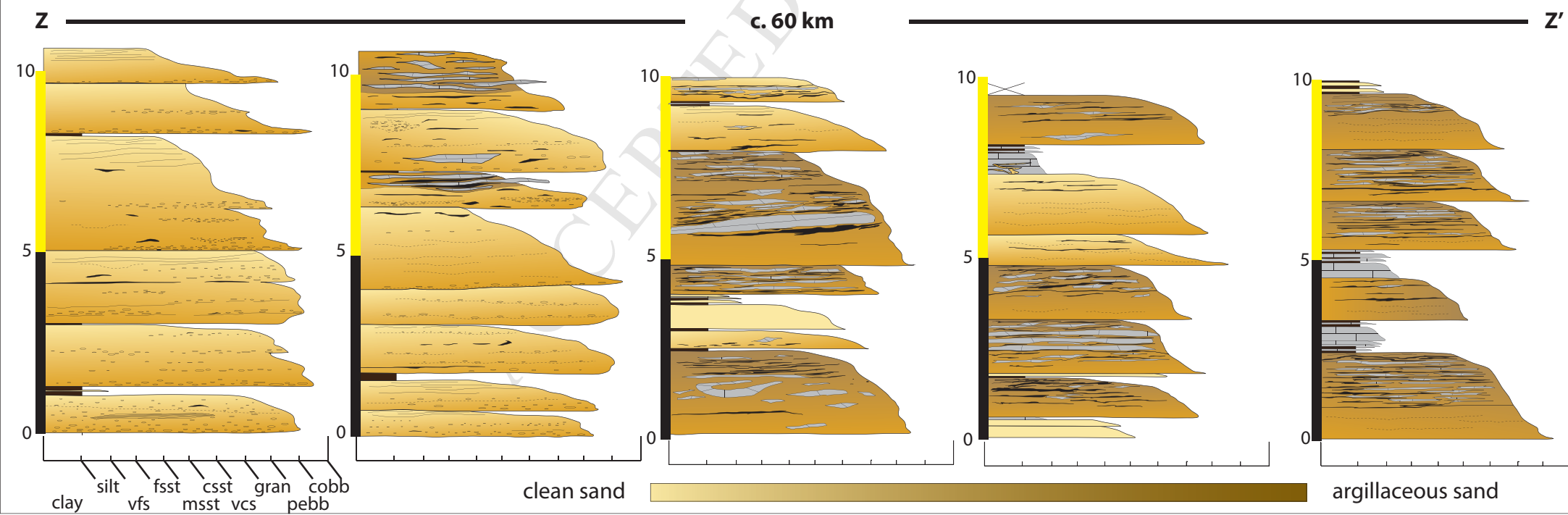
A Idealized Channel FA lateral stacking patterns

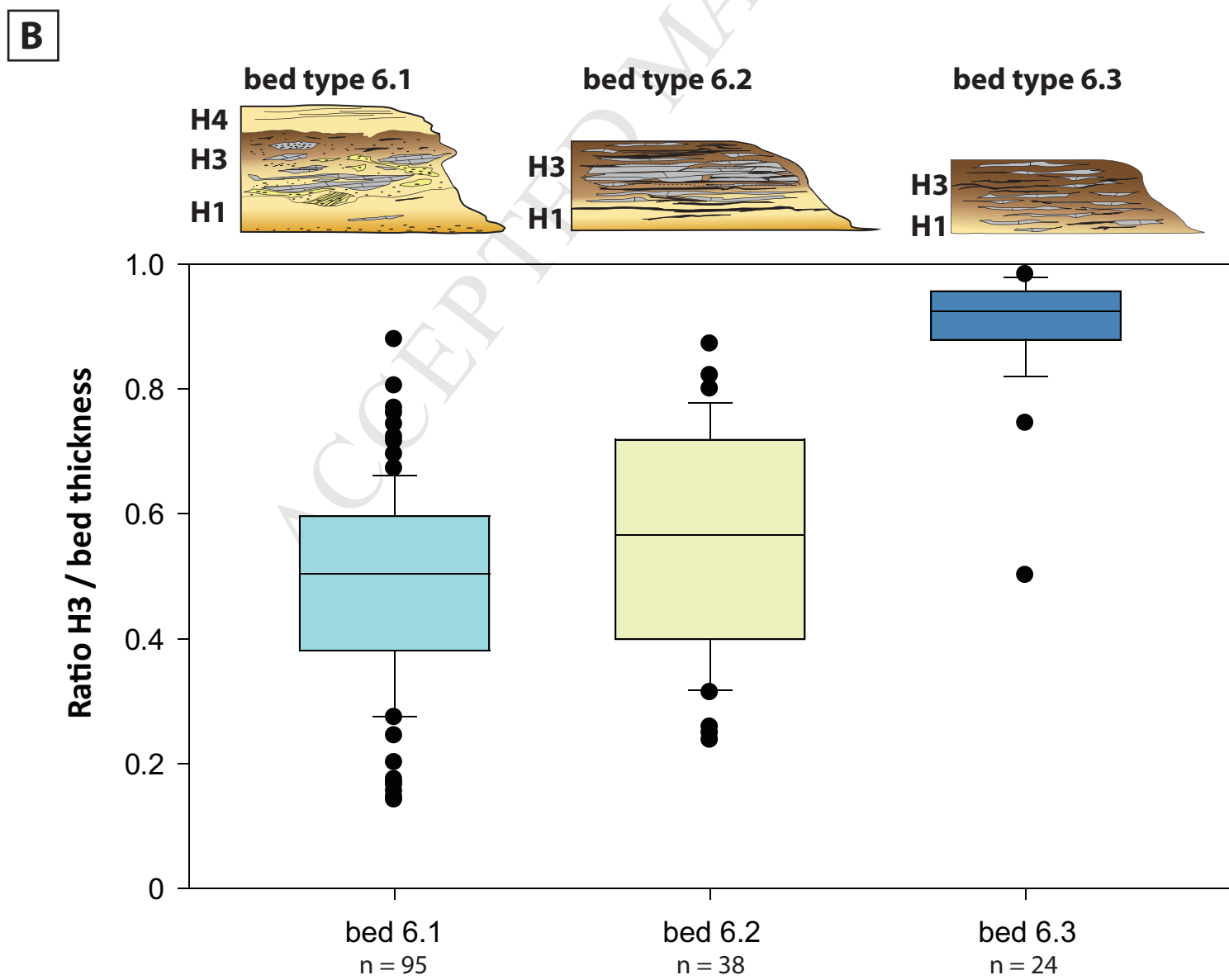
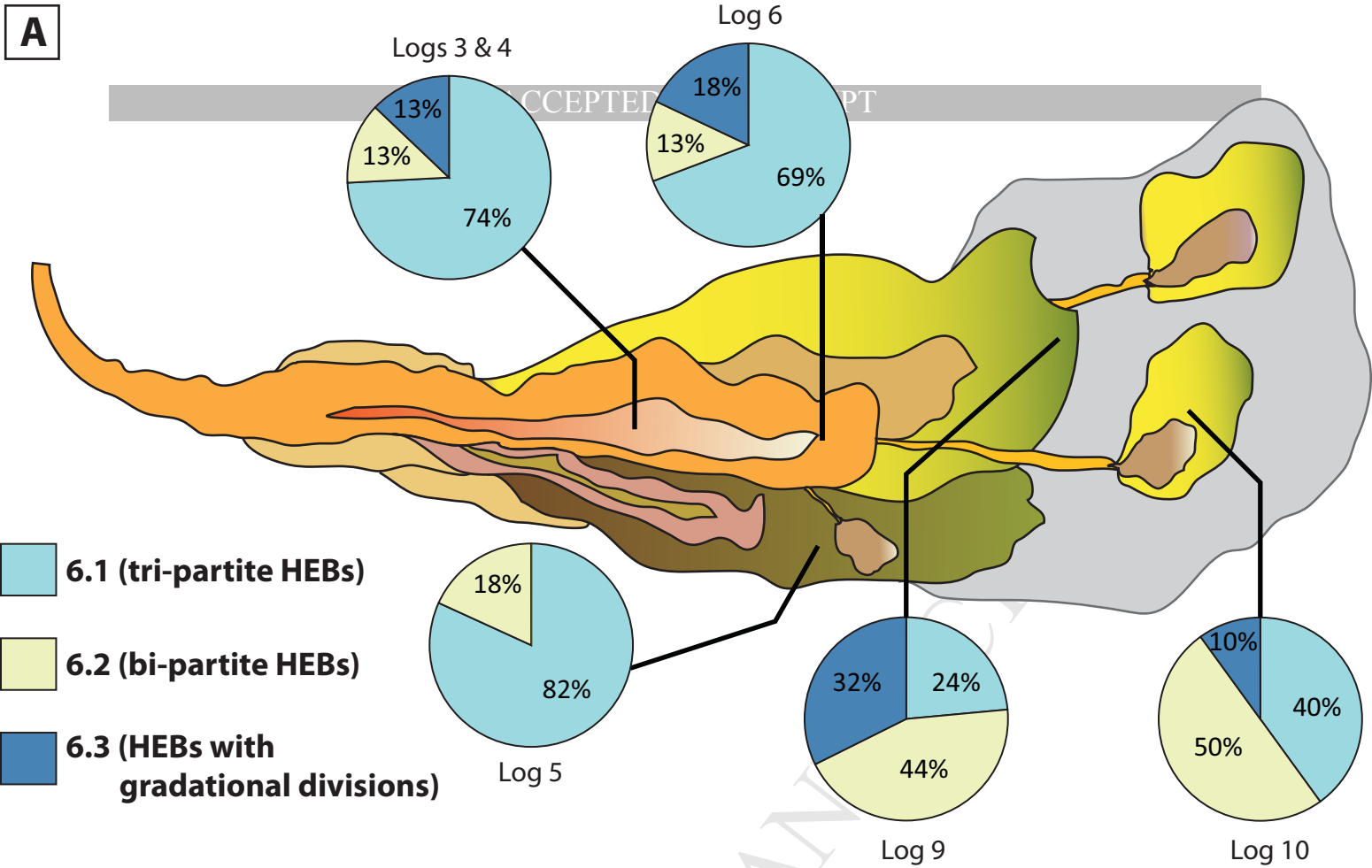


B Idealized Unchanneled BTA lateral stacking patterns



C Idealized down-current axial sediment fairway stacking pattern trends





Highlights

- Multi-scale approach illustrating facies heterogeneity due to hybrid event bed emergence
- Sand-rich turbidite system's characteristics rapidly shift within a short down-dip distance
- Facies heterogeneity occurs at the bed-scale (i.e. sub-seismic scale)
- Idealized down-current and along-current stacking pattern trends for sand-rich HEB-prone turbidite systems are proposed